Evaluating regional emission estimates using the TRACE-P observations

G. R. Carmichael,[1] Y. Tang,[1] G. Kurata,[2] I. Uno,[3] D. G. Streets,[4] N. Thongboonchoo,[1] J.-H. Woo,[1] S. Guttikunda,[1] A. White,[5] T. Wang,[6] D. R. Blake,[7] E. Atlas,[8] A. Fried,[8] B. Potter,[9] M. A. Avery,[10] G. W. Sachse,[10] S. T. Sandholm,[11] Y. Kondo,[12] R. W. Talbot,[13] A. Bandy,[14] D. Thorton,[14] and A. D. Clarke[15]

Received 31 October 2002; revised 25 May 2003; accepted 11 June 2003; published 15 November 2003.

[1] Measurements obtained during the NASA Transport and Chemical Evolution over the Pacific (TRACE-P) experiment are used in conjunction with regional modeling analysis to evaluate emission estimates for Asia. A comparison between the modeled values and the observations is one method to evaluate emissions. Based on such analysis it is concluded that the inventory performs well for the light alkanes, CO, ethyne, SO_2, and NO_x. Furthermore, based on model skill in predicting important photochemical species such as O_3, HCHO, OH, HO_2, and HNO_3, it is found that the emissions inventories are of sufficient quality to support preliminary studies of ozone production. These are important finding in light of the fact that emission estimates for many species (such as speciated NMHCs and BC) for this region have only recently been estimated and are highly uncertain. Using a classification of the measurements built upon trajectory analysis, we compare observed species distributions and ratios of species to those modeled and to ratios estimated from the emissions inventory. It is shown that this technique can reconstruct a spatial distribution of propane/benzene that looks remarkably similar to that calculated from the emissions inventory. A major discrepancy between modeled and observed behavior is found in the Yellow Sea, where modeled values are systematically underpredicted. The integrated analysis suggests that this may be related to an underestimation of emissions from the domestic sector. The emission is further tested by comparing observed and measured species ratios in identified megacity plumes. Many of the model derived ratios (e.g., BC/CO, SO_x/C_2H_2) fall within ~25% of those observed and all fall outside of a factor of 2.5. *INDEX TERMS:* 0305 Atmospheric Composition and Structure: Aerosols and particles (0345, 4801); 0322 Atmospheric Composition and Structure: Constituent sources and sinks; 0345 Atmospheric Composition and Structure: Pollution—urban and regional (0305); 0365 Atmospheric Composition and Structure: Troposphere—composition and chemistry; *KEYWORDS:* emission evaluation, chemical transport model, TRACE-P, biomass burning

Citation: Carmichael, G. R., et al., Evaluating regional emission estimates using the TRACE-P observations, *J. Geophys. Res.*, *108*(D21), 8810, doi:10.1029/2002JD003116, 2003.

[1]Center for Global and Regional Environmental Research, University of Iowa, Iowa City, Iowa, USA.
[2]Department of Ecological Engineering, Toyohashi University of Technology, Toyohashi, Japan.
[3]Research Institute for Applied Mechanics, Kyushu University, Fukuoka, Japan.
[4]Decision and Information Sciences Division, Argonne National Laboratory, Argonne, Illinois, USA.
[5]Department of Chemical Engineering, University of California, Davis, Davis, California, USA.
[6]Department of Civil and Structural Engineering, Hong Kong Polytechnic University, Hong Kong, China.
[7]Department of Chemistry, University of California, Irvine, Irvine, California, USA.
[8]National Center for Atmospheric Research, Boulder, Colorado, USA.
[9]University of Tulsa, Tulsa, Oklahoma, USA.
[10]NASA Langley Research Center, Hampton, Virginia, USA.
[11]Georgia Institute of Technology, Atlanta, Georgia, USA.
[12]Research Center for Advanced Science and Technology, University of Tokyo, Tokyo, Japan.
[13]Institute for the Study of Earth, Oceans, and Space, University of New Hampshire, Durham, New Hampshire, USA.
[14]Chemistry Department, Drexel University, Philadelphia, Pennsylvania, USA.
[15]School of Ocean and Earth Science and Technology, University of Hawaii, Honolulu, Hawaii, USA.

0148-0227/03/2002JD003116$09.00

1. Introduction

[2] Developing accurate emission estimates is critical to atmospheric chemistry studies and to the development of environmental management strategies [*National Research Council* (*NRC*), 1991]. However, quantifying emissions is difficult, as the estimates depend on the quantity and quality of the fuel used, the manner in which it is consumed, and what control technologies are utilized. In developed regions such as North America and Europe, emission estimates have been under development for several decades, and while estimates of certain species are believed to fairly certain (e.g., SO_2 emissions), others still remain problematic (e.g., NMHC from industrial sources). Further complicating the issue is that the chemistry of the atmosphere is controlled by total emissions, so natural emissions such as biogenic emissions, as well as those from biomass burning, must be quantified.

[3] Emission estimates for East Asia have only recently been estimated. A detailed inventory of air pollutant emissions in Asia in the year 2000 has been developed to support atmospheric modeling and analysis of observations taken during the NASA Transport and Chemical Evolution over the Pacific (TRACE-P) mission and Asian Pacific Regional Aerosol Characterization (ACE-Asia) experiment funded by the National Science Foundation (NSF) and the National Oceanic and Atmospheric Administration (NOAA). The details of the inventory development, estimates of uncertainties, and a summary of previous emission estimates are presented by *Streets et al.* [2003a]. These emission estimates are uncertain, and the further refinement and improvement requires their evaluation using observations. Unfortunately, comprehensive measurements of atmospheric composition that can be used to evaluate emission estimates are often lacking.

[4] Measurements obtained during the NASA TRACE-P experiment provide a means to evaluate the quality of the estimated emissions. In this paper we integrate the aircraft measurements with regional-scale modeling techniques to evaluate and characterize regional features of Asian emissions. The standard use of models to assess emissions is to start with an emissions inventory constructed from activity data and emission factors (i.e., a bottom-up approach), then run the model in the forward mode and compare predicted values with the observations, and then attempt to draw inferences about the emissions inventory from the degree of agreement between the predicted and observed values; i.e., emissions → model → predicted-fields → compare predicted with observed → emission inferences.

[5] The sequence can of course be reversed, starting with the observations, and then using the model to estimate the emissions needed in order to have the model predicted fields match (in some optimal manner) the observations (i.e., inverse emissions modeling). The inverted emissions can then be compared with the a priori (bottom-up) estimate and inferences drawn [e.g., *Kasibhatla et al.*, 2002; *Palmer et al.*, 2003]. In this paper we explore additional ways to combine observations and models in an attempt to infer additional information about the quality of estimated Asian emissions.

[6] The paper is structured as follows. In section 2 the analysis methods used are described. We then compare the calculated concentrations using the estimated emissions with the aircraft observations (section 3.1). This provides a general assessment of the ability of the inventory to represent the observed trace gas distributions. In sections 3.2–3.4, trajectory analysis techniques are used to classify the observations by source region and, along with the observations, used to reconstruct spatial distributions of trace species. Results from this analysis are compared with model-derived values and to regional estimates of emissions. This analysis provides additional insights into regional features and identifies areas where the emissions inventory may be deficient. In section 3.5 the emissions are further tested by comparing observed and measured species ratios in identified megacity plumes. The paper concludes with a summary of major findings and a discussion of how the analysis can be extended to further evaluate and enhance the quality of emission estimates.

2. Analysis Methodology

[7] In this paper results from the regional model, CFORS/STEM-2K1, are used to evaluate the emission estimates and to characterize regional features. CFORS is a multitracer, online system built within the RAMS mesoscale meteorological model [*Pielke et al.*, 1992]. An important feature of CFORS is that multiple tracers are run online in RAMS so that all the online meteorological information such as three-dimensional (3-D) winds, boundary-layer turbulence, surface fluxes, and precipitation amount are directly used by the tracer model at every time step. As a result, CFORS produces with high time resolution 3-D fields of tracer distributions and major meteorological parameters. An important aspect of the CFORS system is that emissions evaluation and analysis are intimately coupled to the modeling activities. CFORS includes a wide variety of tracers to help characterize air masses. These include (1) important anthropogenic species (SO_2/SO_4, CO, black carbon, organic carbon, fast and slow reacting hydrocarbons, and NO_x); (2) species of natural origin (yellow sand, sea salt, radon, volcanic SO_2); and (3) markers for biomass burning (CO, black carbon, and organic carbon). In the analysis of the TRACE-P observations, the CFORS system was applied in hind cast mode using ECMWF global meteorological data set (6 hour interval with $1^\circ \times 1^\circ$ resolution), analyzed weekly SST (sea surface temperature) data, and observed monthly snow-cover information as the boundary conditions for the RAMS calculations.

[8] The meteorological fields and those emissions estimated in an online manner inside of CFORS were used to drive the STEM-2K1 comprehensive chemical transport model (CTM), which then produced estimated fields of primary and secondary chemical and aerosol constituents. The important new features in STEM-2K1 include: (1) the use of the SAPRC99 chemical mechanism [*Carter*, 2000], which consists of 93 species and 225 reactions; (2) the integration of the chemical mechanism using and the implicit second-order Rosenbrock method [*Verwer et al.*, 1999]; (3) the calculation of photolysis rates online, considering the influences of cloud, aerosol, and gas-phase absorptions due to O_3, SO_2, and NO_2, using the NCAR Tropospheric Ultraviolet-Visible (TUV) radiation model

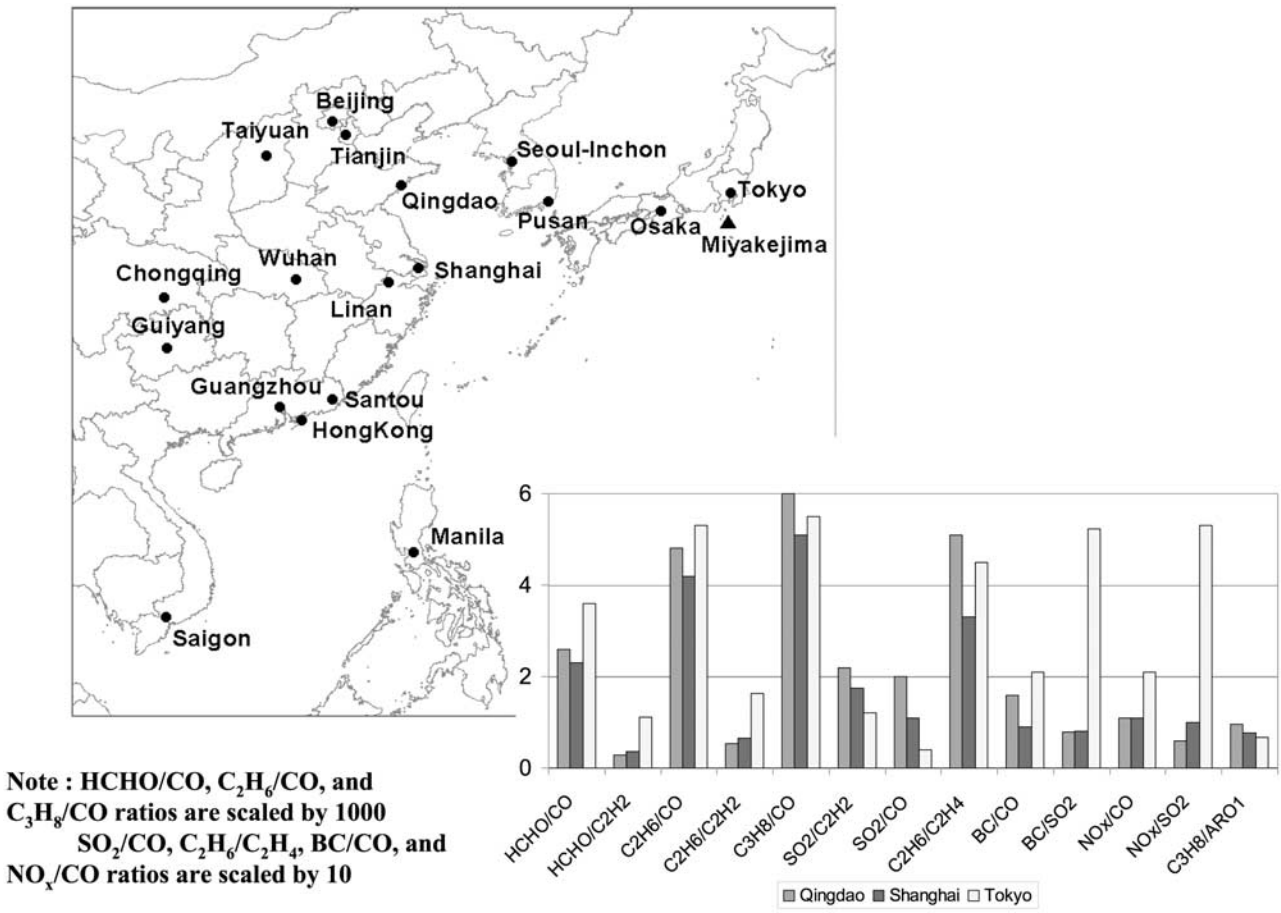

Figure 1. Domain used in the emissions and modeling analysis. Also shown are the locations of the megacities and the Miyakejima volcano. Emission ratios (molar) for a variety of species used in the analysis for Shanghai, Tokyo and Qingdao are also shown. See color version of this figure at back of this issue.

[*Madronich and Flocke*, 1999]; and (4) the extension of the aerosol calculations to include optical information (e.g., extinction) in addition to mass, size, and composition. Details regarding the radiative transfer calculations are presented by *Tang et al.* [2003a]. Complete details regarding the model used can be found in the works of *Uno et al.* [2002] and *Carmichael et al.* [2003].

[9] The anthropogenic emission inventories (SO_x, NO_x, CO, CO_2, NH_3, black carbon, organic carbon, and hydrocarbons) used in this paper were prepared specifically for the TRACE-P and ACE-Asia experiments. A unique aspect of this bottom-up inventory is that it is driven by regional-specific information on fuels and activity. Biofuels and fossil fuels can be tracked separately, as can emissions from various economic sectors (e.g., domestic, transport, power generation, industrial). Emissions from specific regions (administrative units where specific activity and fuel data were collected) and even megacities can be isolated. The details of the inventory are presented by *Streets et al.* [2003a] and *Woo et al.* [2003]. Another important source of aerosols and trace gases in the springtime in Asia is biomass burning. Daily averaged CO, BC, and OC emission estimates were prepared based on the analysis of daily AVHRR fire counts as discussed by *Streets et al.* [2003a] and *Woo et al.* [2003]. Volcanoes are one of the major sources of sulfur dioxide in Asia. Estimated volcanic SO_2 emission for the major active volcanoes within the modeling domain are included in the analysis. During TRACE-P, large quantities of SO_2 were emitted (as much as 10 million ton-SO_2/year) from the Miyakejima Island (Mt. Oyama) just south of Tokyo [*Yoshino et al.*, 2002]. Figure 1 shows the CFORS/STEM-2K1 domain of analysis, along with the megacities included in the analysis. Also shown are the emission ratios of various species for Shanghai, Tokyo, and Qingdao. There is significant regional variability in the estimated emissions, which reflects local economic activity and emission control technology. In this paper we explore ways to utilize the TRACE-P observations, along with the models, to identify and evaluate these regional emission signals.

[10] Various analyses were performed in the evaluation of emissions. One approach was to directly compare results from model simulations using our estimated emissions with the aircraft observations. For these comparisons the model was sampled along 12 DC-8 and 12 P-3B flight paths at 5-min intervals and compared with the measured values in the 5-min merged data set (~2200 points). The merged data set consists of all measurements taken on the aircraft combined together in a single data set with common and uniform time intervals and consistent formats. Model results

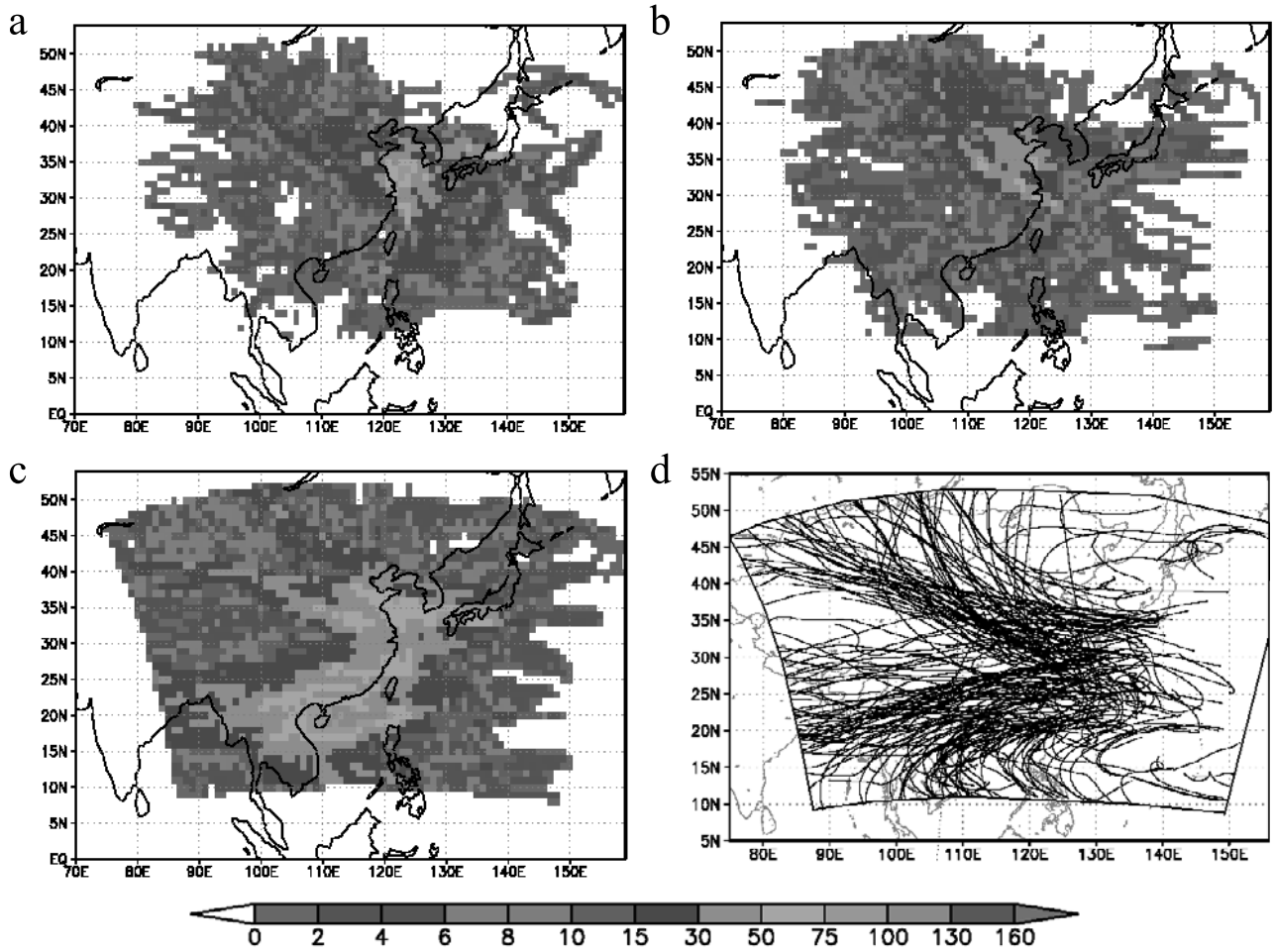

Figure 2. Trajectory statistics for 5-day back-trajectories calculated for every 5-min flight segment along the 12 DC-8 (4 March to 1 April) and 12 P-3B (4 March to 2 April) flights. Shown are the number of times the back-trajectories passed over each $1^\circ \times 1^\circ$ grid cells below 1.5 km (a), between 1.5 and 3 km (b), over 3 km (c). Sample trajectories are shown in Figure 2d, which include ~2200 trajectories. See color version of this figure at back of this issue.

were interpolated to the exact times and locations of the aircraft measurements. Since the model results are driven by the emissions, the degree of agreement between the modeled values and the observations provides an evaluation of the emissions. If the model were perfect (and of course it is not), then this comparison would provide a direct test of the emissions, and agreement would imply that the emissions are quantitatively correct, and disagreement would indicate errors in the emissions. In practice models are imperfect, so disagreements (as well as agreements) are a convoluted combination of model, measurement, and emission errors. In this paper the comparisons were restricted to observations below 2 km in order to maximize the influence of the local sources and to minimize the impacts of model deficiencies associated with where and when the air mass was lifted by convection, and errors associated with the location and timing of biomass emissions. As discussed by *Kiley et al.* [2003], the most significant differences between results calculated by the seven CTMs used during TRACE-P and the observations occurred in outflow regions above ~2 km.

[11] The second approach was to classify the aircraft measurements by source region using trajectory analysis. Back-trajectories were calculated every 5 min along the flight paths using the 3-D RAMS meteorological fields, and the number of times the trajectories passed over specific regions of interest were counted (see Figure 2). For emissions-related comparisons, the analysis was limited to locations along the back-trajectories that were within 2 km of the surface, since these are the air masses most likely to be influenced by the regional emissions. The statistics arising from this analysis for all flights using 5-day back-trajectories are presented in Figure 2. These data were further classified for specific analysis. For example, for studying megacity emissions, the data were further classified into measurement periods under influence of emissions from specific megacities. These results are presented in Figure 3. This analysis also provides an estimate of the time along the back trajectory since the air mass encountered the urban environment. This analysis identified many opportunities to characterize emissions from large cities. For example, air masses that passed over Shanghai were identified more than 170 times, and ~90 of these had travel times of less than 1 day. Please note that all encounters along the back-trajectory were counted and that a single

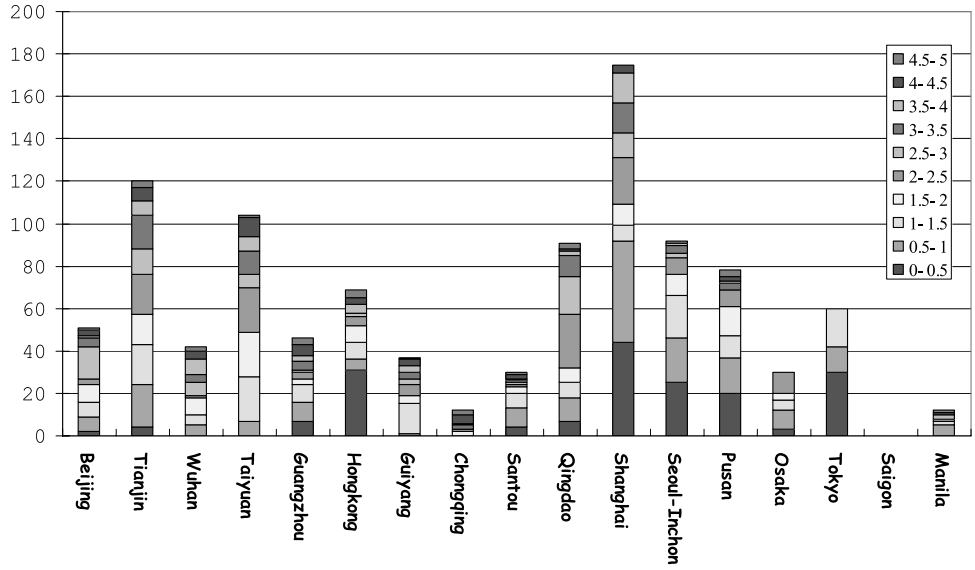

Figure 3. Trajectory statistics for 5-day back-trajectories calculated for every 5-min flight segment along the 12 DC-8 and 12 P-3B flights. Shown are the number of times the back-trajectories passed over selected megacities at altitudes below 2 km, classified by the age of the air mass (days). Emission ratios (molar) for a variety of species used in the analysis for Shanghai, Tokyo, and Qingdao are also shown. See color version of this figure at back of this issue.

back-trajectory could encounter more than one designated city (but not at the same time). Using this classification of the measurements, observed species distributions and ratios of species were compared with those modeled and to ratios estimated from the emissions inventory.

3. Results and Discussion

3.1. Mission-Wide Results

[12] A comprehensive comparison of all the modeled results with observed values during TRACE-P is presented by *Carmichael et al.* [2003]. The details of this analysis are not repeated here. However, a comparison of the observations taken at flight altitudes below 2 km with calculated values is presented in Table 1. Most mean values calculated by the model were within ~±30% of the observed values for all the parameters shown. A comprehensive comparison of modeled results with observed values during TRACE-P is presented by *Carmichael et al.* [2003]. The results in Table 1, along with those presented by *Carmichael et al.* [2003], show that the model performs well for the light alkanes, CO, ethyne, SO_2, and NO_x. Furthermore, based on model skill (as measured by means and correlation coefficients) in predicting important photochemical species such as O_3, HCHO, OH, HO_2, and HNO_3, it is concluded that the emission inventories are of sufficient quality to support preliminary studies of ozone production. These are important findings in light of the fact that emission estimates for many species (such as speciated NMHCs and BC) for this region have only recently been estimated and are highly uncertain [c.f. *Streets et al.*, 2003a, and references therein]. The uncertainty of these emissions was estimated by error analysis of each emitting subsector and by combining the coefficients of variation (CV, or the standard deviation divided by the mean) of the contributing factors. The estimated overall uncertainty in emissions for all of Asia, ranked in increasing order of uncertainty and measured as 95% confidence intervals are: ±16% (SO_2), ± 31% (CO_2), ±37% (NO_x), ±65% (CH_4), ±72% (NH_3), ± 130% (NMVOC), ±185% (CO), ±360% (BC), and ±450% (OC). However, while the model results clearly encompass the observations when these uncertainties are taken into consideration, it is important to note that the model can at best explain only ~65% of the variability seen in the observations. This inability to explain the variability is due in part to inventory deficiencies in magnitude and/or spatial and temporal distributions. Below, additional ways to combine observations together with the model information to further test various aspects of the emissions inventory are explored.

3.2. Regional Emission Signals

[13] Asian emissions show strong regional differences as discussed by *Woo et al.* [2003]. These differences reflect in large part differences in the contribution of fossil fuels, biofuels, and biomass (open) burning. This can be illustrated by looking at ratios of various species. One example is shown in Figure 4, where propane to benzene ratios (moles of propane emitted in March/moles of benzene emitted in March) calculated from the total emissions are presented. The emissions show a strong south to north gradient in this ratio, with low values indicating regions with large biomass burning sources, intermediate values reflecting a blend of biomass and biofuel usage, and the largest values reflecting highly industrial regions dominated by fossil fuel usage.

[14] Propane and benzene have similar loss rates against reaction with OH [*Carter*, 2000] and are inefficiently removed by wet removal processes; thus changes in their ratio should reflect most strongly differences in emissions. Under these conditions, then the aircraft measurements can be used to back-calculate regional distributions. To test this hypothesis 5-day back-trajectories were calculated using the three-dimensional RAMS-derived meteorological fields for

Table 1. Observed and STEM-Simulated Mean Values and Correlation Coefficients (R) for TRACE-P DC-8 Flights 6 to 17 and P-3 Flights 8 to 19 for Flight Altitudes Below 2 km[a]

	DC-8 Flights 6–17			P3 Flights 8–19		
Chemical Species	Observed	Modeled	R	Observed	Modeled	R
CO, ppbv	219	203	0.73	229	219	0.68
O_3, ppbv	51	52	0.80	55	56	0.88
Ethane, ppbv	2.0	1.6	0.88	2.0	1.7	0.68
Propane, ppbv	0.62	0.46	0.81	0.65	0.50	0.62
Ethyne, ppbv	0.78	0.63	0.69	0.74	0.67	0.62
Ethene, ppbv	0.18	0.20	0.61	0.14	0.13	0.52
SO_2, ppbv	1.55	1.04	0.43	1.6	2.5	0.77
NO_2, ppbv	0.27	0.25	0.24	0.52	0.41	0.23
NO, ppbv	0.035	0.041	0.22	0.080	0.078	0.11
HNO_3, ppbv	0.61	0.73	0.74	0.35	0.90	0.22
OH, pptv	0.11	0.11	0.75	0.21	0.13	0.59
HO_2, pptv	10.8	10.9	0.79	15.5	12.6	0.66
Benzene + Toluene, ppbv	0.33	0.19	0.64	0.28	0.15	0.41
HCHO, ppbv	0.60	0.59	0.68	N/A	N/A	N/A
BC, ug/std m^3	0.84	0.67	0.65	N/A	N/A	N/A

[a]Analysis based on ~300 data points for DC-8 flights and ~465 for P-3 flights.

each 5-min segment of the DC-8 and P-3B flights and the trajectories classified according to the propane to benzene ratio. For each trajectory it was assumed that the observed value of propane/benzene for that time period remained constant for the entire path along the trajectory, and that each grid cell where the trajectory passed below 2 km was assigned this value. The spatial distribution of propane/benzene when each grid cell was averaged over all flights is presented in Figure 4b. The reconstructed distribution based on observations looks very similar to that calculated from the emissions inventory (Figure 4a), and the reconstruction captures the dominant regional signals. The results presented in Figure 4 are shown in terms of the administrative regions used in compiling emission inventories. For subsequent use in modeling analysis, the emissions within a region were allocated to a finer spatial grid (1° by 1°) using surrogate data (e.g., population distributions) as discussed by *Woo et al.* [2003]. The trajectory analysis was performed on this finer grid and then values averaged within the region to produce the results shown in Figure 4b.

[15] There are some peculiarities associated with this analysis. By the nature of the analysis, only the largest signals are captured. For example the Hong Kong and Taiwan signals are not retrieved as they are surrounded by large regions with higher absolute emissions with lower propane/benzene values. For the same reasons trajectories in the direction of Beijing pick up the large signal from this region but assign this same value to all trajectories as they move farther to the west, leading to an overestimation of the ratios in the western provinces. Similarly, for the Philippines there are few trajectories that pass over this country (see Figure 2), and those that do also tend to have passed over Hong Kong and surrounding areas and thus have been imprinted with the higher emission ratios. These aspects of the analysis could be improved by restricting the analysis to 2 or 3-day back trajectories and adding some a priori

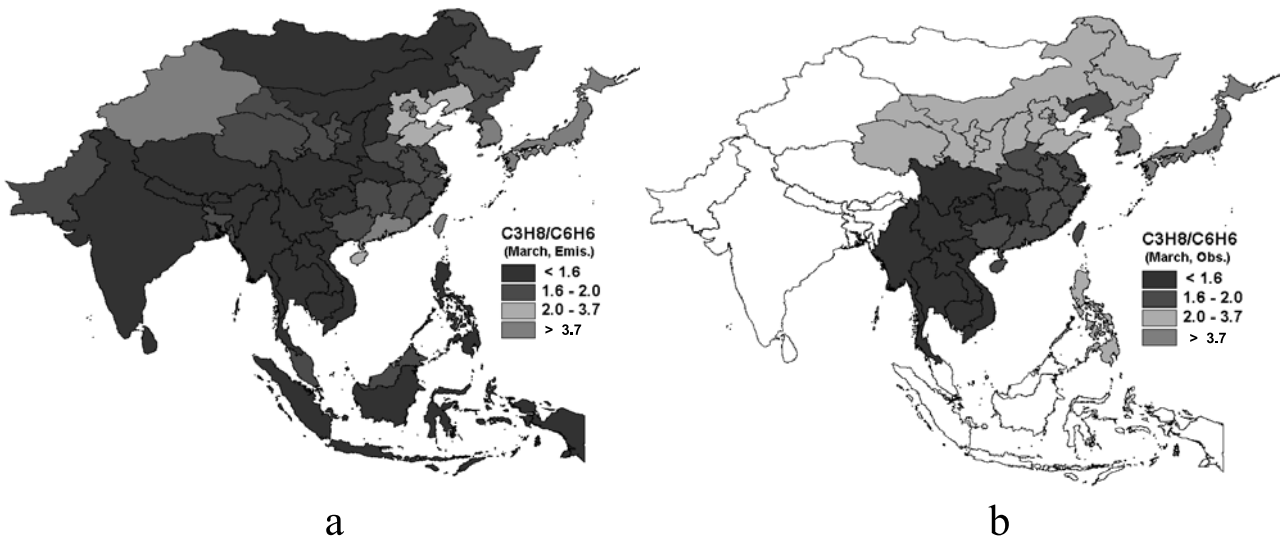

Figure 4. The regional distribution of propane to benzene ratio (molar) determined from the emissions inventory (a) and by back-trajectory analysis using the ratios observed onboard the aircrafts in all flights (b). See color version of this figure at back of this issue.

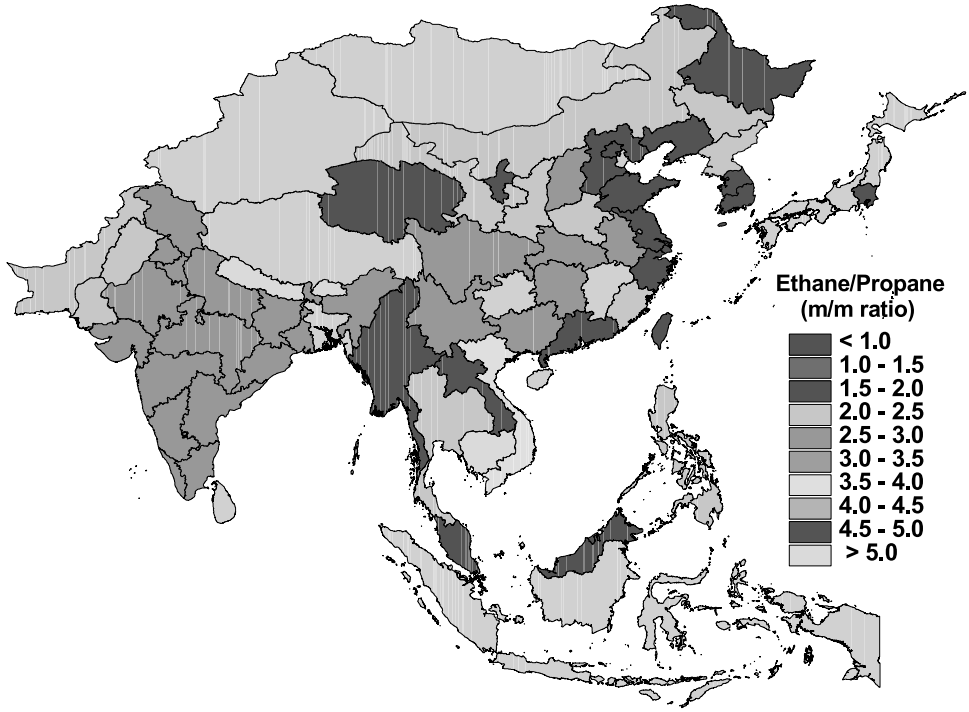

Figure 5. The regional distribution of ethane to propane ratios (molar) determined from the emissions inventory. See color version of this figure at back of this issue.

information, such as population density, to help further classify the trajectory segments used in the reconstruction. Furthermore, this analysis works best using ratios of species with similar chemical reaction loss rates with respect to OH and that have some degree of spatial homogeneity within regions, as mixing effects as well as differences in reaction rates, result in changes in the ratio along the trajectory. This is discussed in more detail later.

[16] The regional variation in the ratios contains important information about source categories. For example the ethane/propane ratios in the total emissions in Asia vary from $\sim$1–6 (Figure 5). The ethane/propane values for specific emission categories also vary significantly, as shown in Table 2. Biomass burning in SE Asia has a value of 8, biofuel combustion 2.3, and transportation 0.5. The importance of these activities is reflected in the aggregated regional emissions. SE Asia has the largest value reflecting the dominant role of biomass burning [*Tang et al.*, 2003b]. The importance of biofuels in Central China and the dominating role of industrial and transportation in South Korea and Japan are also clearly depicted in the regional emissions.

[17] The observed relationship between ethane and propane for the DC-8 and P-3B flights are shown in Figure 6, along with the predicted values. As discussed previously and shown in Table 1, the model is able to accurately estimate the ambient levels of ethane and propane. However, when viewed together, the model predicts a much more linear relationship than that observed. The trajectory analysis indicates that many of the low values are associated with

Table 2. Emission Factor Ratios (Mass Basis) for Various Source Sectors[a]

	Emission Factor Ratios (Full MW Basis)					
	Biomass Burning (SE Asia)[b]	Biomass Burning (Local/China)[c]	Biofuel Use[d]	Industry and Power[e]	Domestic (Coal, Oil, and Biofuel)[f]	Transport[g]
CO	693	657	289	61	652	270
SO_2	3.8	2.9	1	103	26	7.5
Ethane	8	6.9	4.4	1.5	1	1.1
Propane	1	3.7	1.9	2	2.8	2.2
Ethene	13	10	6.7	1	19	5.5
Benzene	2.7	1	7	1.4	8.8	1

[a]For example, for the transport sector there is 270 times more CO emitted than benzene. The emission factor ratios are estimated across all of Asia, except where indicated (biomass burning). Values calculated by taking the ratios of emission factors (e.g., for biomass burning [CO-emitted/kg fuel burned]/[Propane-emitted/kg-fuel burned].
[b]Based on *Andreae and Merlet* for tropical forests; good for Southeast Asia forest burning.
[c]Based on *Andreae and Merlet* for agricultural waste burning; good for local burning in China, such as Lin'an.
[d]Based on *Andreae and Merlet* for biofuel burning; good for local biofuel use in China.
[e]Based on total emissions for power plants and industrial facilities (combined).
[f]Includes all residential activities from all fuel types, paints, and solvents.
[g]Includes all fuel combustion by vehicles but not refineries, etc.

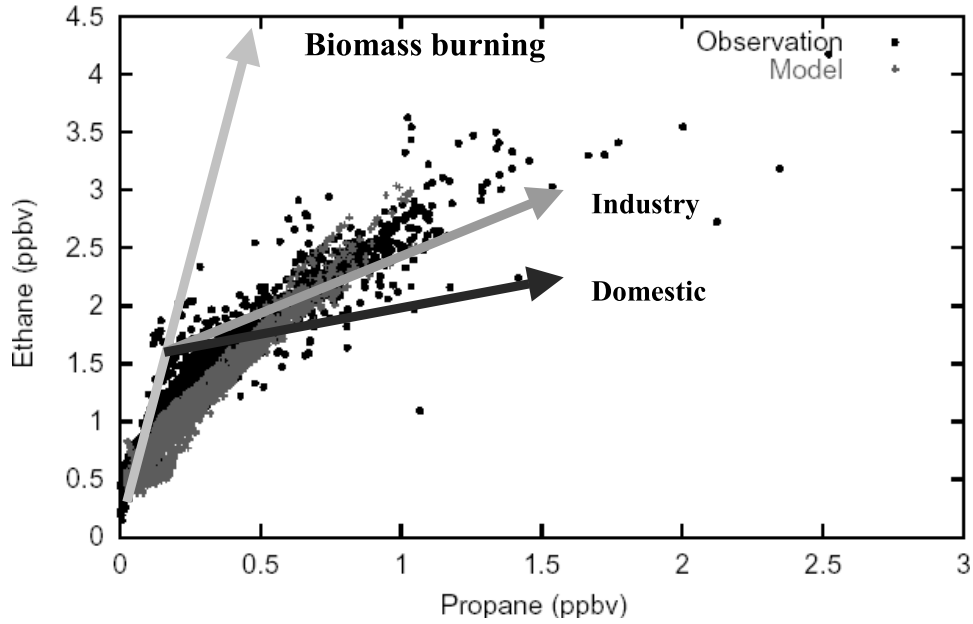

Figure 6. Observed and modeled relation between ethane to propane for the 5-min segments of the P-3B and DC-8 flights. Colored arrows show emission ratio for various sources categories. See color version of this figure at back of this issue.

trajectories from SE Asia. These results suggest that biomass-burning emissions in SE Asia may be underestimated or that the emission factors for ethane and propane (and other NMHC species) for biomass burning in SE Asia may be different from those used to build the emissions inventory. As discussed previously and as reflected in the uncertainty in the emission estimates, additional information on emission factors and burning activity in SE Asia is needed in order to improve biomass-burning emissions. Furthermore, inferring information about biomass burning from SE Asia using the Trace-P data is a challenge as the air masses from this region were 3–5 days old by the time they were observed. Dilution of the biomass signals, mixing with other sources, and errors in trajectories, all add to the uncertainties. Nonetheless, results presented in this paper, as well as chemical mass balance analysis using this data set [*Woo et al.*, 2003] suggest that useful information regarding biomass emissions can be obtained from the Trace-P data.

3.3. Observation-Based Reconstruction of Concentration Fields

[18] Further insights into the relationship between emissions and the observed-modeled behavior can be seen by looking at scatter-plots of the predicted and observed CO, as shown in Figure 7. All data points from the 5-min merged data sets for the DC-8 and P-3B for East Asia flights are shown. The points identified in red are measurements with CO > 400 ppbv, and the back-trajectories associated with these data points are also shown. Most of the CO > 400 ppbv points are associated with westerly winds and descending trajectories that passed over east-central China before traveling into the Yellow Sea. For these trajectories the model systematically underpredicts (not only CO, but ethyne, ethane, BC, etc.). The underprediction of CO concentrations at low altitudes in the Yellow Sea is an important observation and is also seen in a variety of global and regional models used in TRACE-P analysis [see *Kiley et al.*, 2003]. These very high values are associated with distinct plume-like features, which are not resolved in models using an 80 km grid resolution. To study the effect of model resolution, calculations were also performed using a 16 km horizontal grid spacing. These calculations showed that resolution could have a big impact on species that are emitted from large point sources (such as NO_x and SO_2). However, there is little CO emitted from large points sources such as those related to power generation, and the increased resolution did not significantly improve the CO calculations in this region. So it is necessary to investigate whether this under-prediction of CO in the Yellow Sea reflects inaccuracies in the emissions.

[19] The average values of the observed CO for flight altitudes below 2 km are also shown (Figure 8a), along with the model calculated monthly averaged CO distribution for the lowest 2 km (Figure 8b). It is important to point out the differences between these plots. The values shown in Figure 8a were calculated by binning the observed data into a spatial (horizontal and vertical) grid and then averaging all the observed values (for the heights below 2 km). The modeled derived fields (0–2 km) shown in Figure 8b are the monthly mean distributions based on averaging all values time periods within the month (and not just times when there was an aircraft observation). Clear differences are seen between the monthly mean and the mission-averaged CO values in the Yellow Sea. These reflect the fact that the aircraft missions selectively sampled outflow associated with strong frontal activity. These events have the highest concentrations but occur with synoptic frequency (every 3–5 days).

[20] Using the back-trajectory technique discussed previously, the spatial distributions of various species were reconstructed using the aircraft observed species concentrations. The spatial distribution of observed CO when each

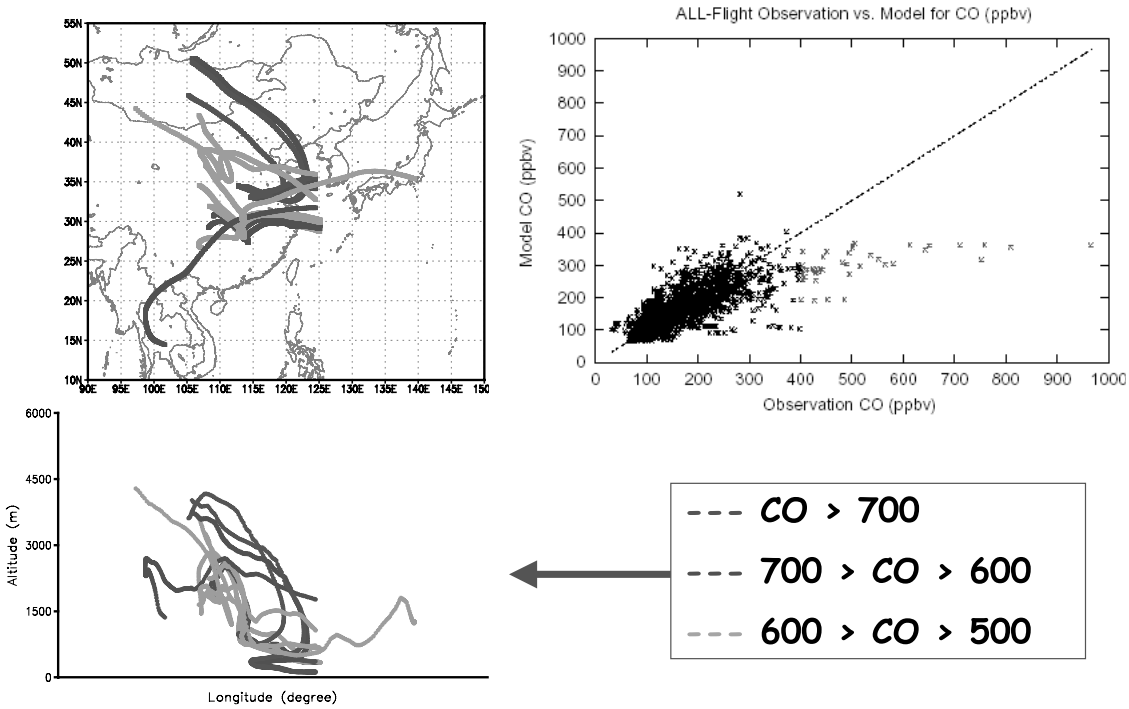

Figure 7. Modeled and observed CO for the DC-8 and P-3B flights (5-min merged data set). The red points indicate data points for which back-trajectories were calculated. The trajectories for the points with CO > 500 ppb are shown (left) and color-coded according to measured CO values. See color version of this figure at back of this issue.

grid cell was averaged over all flights is presented in Figure 8c. Shown are results for each 80 km horizontal grid used in the meteorological and chemical models. The observation-based reconstructed CO field displays many of the important features that appear in the model calculated monthly averaged fields (Figure 8b). This comparison between the observation-based reconstruction and results from the forward model run of the CTM provides an additional evaluation of the emissions. In this comparison both approaches used the same meteorological fields, so differences in the distributions should reflect discrepancies between the estimated and actual magnitude and/or spatial distribution of the emissions. In both fields the highest values are from air masses associated with the biomass burning areas of Southeast Asia, the biomass and fossil fuel regions of central China, and the industrial regions between Shanghai and Beijing. To quantify this analysis, a model-based CO distribution was reconstructed using the calculated values along the flight paths instead of the observations. The mean bias between the model and the observation-based reconstruction is shown in Figure 8d. Interesting patterns emerge. For example, there are widespread regions of good agreement (biases less than ±30 ppb). There is also a pattern of high and low bias in the biomass-burning region of SE Asia. This pattern reflects subregional inaccuracies in the spatial and temporal distribution of biomass burning emissions and inadequacies in model transport associated with convective lifting and orographic effects in this region. The subregional patterns in biomass burning in SE Asia are highly uncertain as discussed by *Woo et al.* [2003]. A persistent negative (underprediction) bias for CO shows up in Central China between Chongqing and Shanghai. This region is one with large estimated emissions, and this region will be discussed in more detail later.

[21] The analysis was repeated for many species. The SO_2 results are shown in Figure 9. Shown are regions dominated by coal use in the large cities in China, and areas impacted by the large sulfur emissions from the Miyakejima volcano located south of Tokyo [*Yoshino et al.*, 2002]. It should be noted that the absolute values of SO_2 reconstructed using the aircraft observations in this manner are low over China because oxidation and deposition reduce its concentration as it travels from the source region to the aircraft. Biomass emissions of SO_2 are small compared with CO, so SO_2 levels in SE Asia are relatively low. Large negative biases are again found in Central China. Negative biases in this region were also found for many other species including BC and ethyne. The large positive bias around Tokyo suggests that the emission estimates from the Miyakejima volcano may be too large. The Miyakejima plume encountered by TRACE-P flights is fresher than continental outflows, so this plume concentration tends to be less affected by SO_2 destruction and depositions comparing to the strong source.

3.4. Central China and Domestic Emissions

[22] The above analysis suggests that emissions in central China may be underestimated in the current emissions. Additional insights can be found by using surface measurements in this region. At the Lin'an surface measurement site (see Figure 1), CO, SO_2, O_3, NO, NO_y, and NMHC were measured for ~2 years, including during the period of TRACE-P [*Wang et al.*, 2001, 2002]. Lin'an persistently

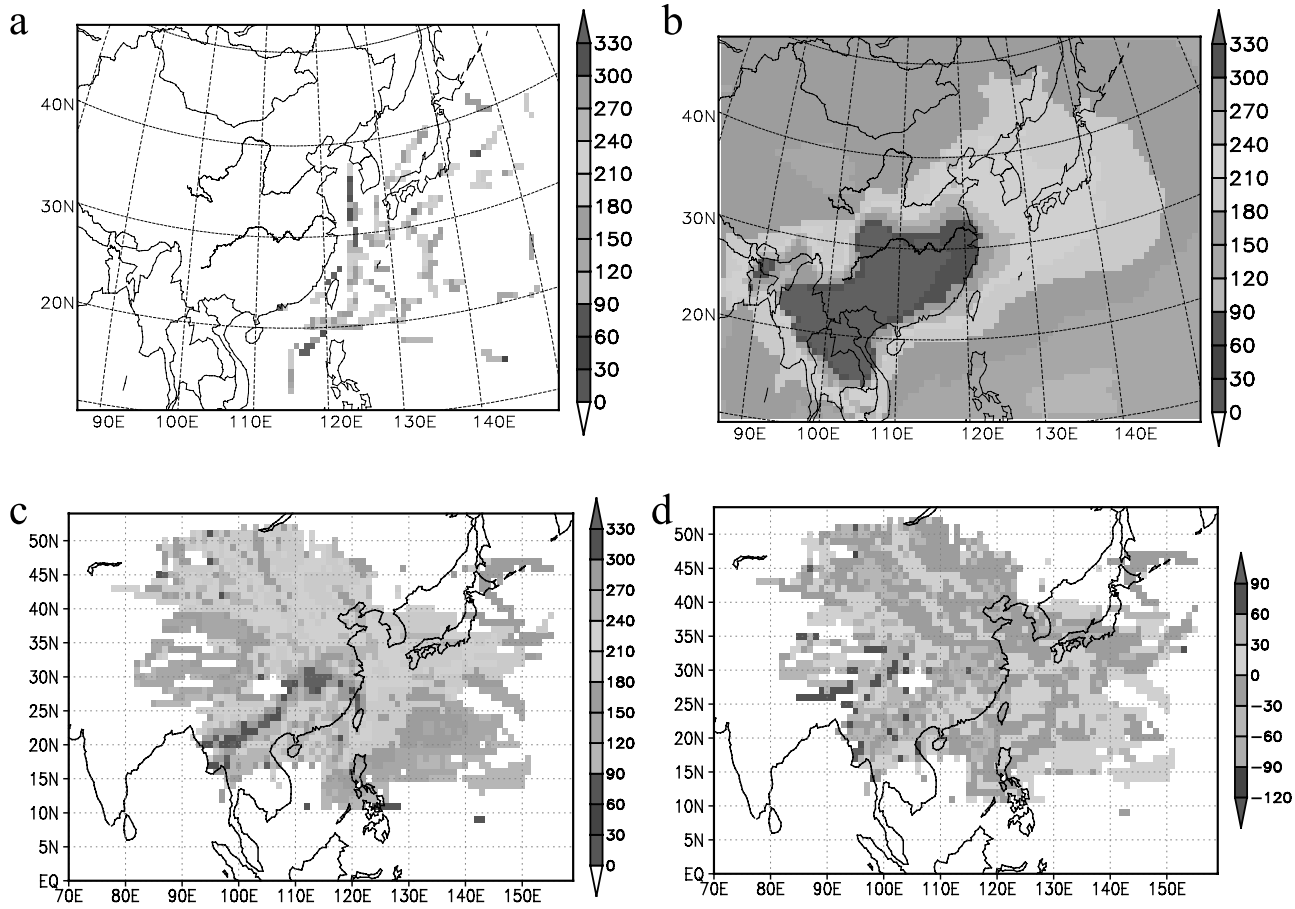

Figure 8. Mission-averaged distributions of CO. Averaged values of aircraft observation for altitudes below 2 km (a); model calculated values for all day-time points in the month of March for altitudes below 2 km (b); average distribution below 2 km reconstructed using the aircraft observed values and back-trajectory analysis (c); and mean monthly bias below 2 km between the reconstructed distribution based on the observations and the distribution reconstructed using the modeled values along the flight path (d). All values are in ppbv. See color version of this figure at back of this issue.

observed very high concentrations as shown in Table 3, where a summary of the calculated and observed surface values at Lin'an for the TRACE-P period are presented. In the mean, the model underestimates CO by a factor of 2 and SO_2 and NO_y by a factor of 3. However, the observed and model slopes of SO_2/CO are quite consistent, while the modeled SO_2/NO_y is 1.7 times higher than the observed value.

[23] Errors in the inventory could be related to region-specific issues such as problems in activity reporting, or inaccuracies in fuel characteristics (which we have no way of checking at this stage of the analysis), or they may reflect a systematic problem within a given sector. The domestic sector is a likely candidate, as its regional importance is focused in central China as shown in Figure 10. Further details regarding emissions from the domestic sector are presented in Table 4. As shown, the relative importance of biofuel and fossil fuel in the domestic sector changes by species. BC is dominated by biofuel, CO is evenly split between fossil and biofuel, and SO_2 is dominated by fossil fuel usage. In central China the fossil fuel usage in the domestic sector is dominated by coal. In the *Streets et al.* [2003b] inventory, the energy scenario used for the year 2000 reflects the recent decline in coal usage and an improvement in the coal quality. The reasons for these trends are discussed in detail by *Streets et al.* [2003b]. However, it is possible that these positive changes did not extend equally across all sectors and that the assumptions about the rate at which the domestic sector was transformed to gas and electricity were too optimistic. If one assumes that the domestic sector usage of coal since 1995 did not change, then the domestic sector emissions would be about double those used in the base-line TRACE-P inventory.

[24] To investigate further the impact of the domestic sector on the calculated distributions, a new simulation was performed in which the domestic sector emissions (only) were doubled. The results are shown in Figure 11, and they show the intriguing feature that the largest increases in concentrations occur preferentially over Central China, and in the Yellow Sea, in a latitude band coincident to where the under predictions occur. The average changes in the Yellow Sea are ~30–40 ppb in the case of CO, but in specific outflow events can be 60 to 100 ppb (as shown for DC-8 flight 9). In the case of BC, doubling the domestic-sector emissions resulted in increased BC levels in the Yellow Sea by as much as a factor of 2. Surface values of CO at Lin'an increased by ~100 ppb for the double domestic-sector simulation.

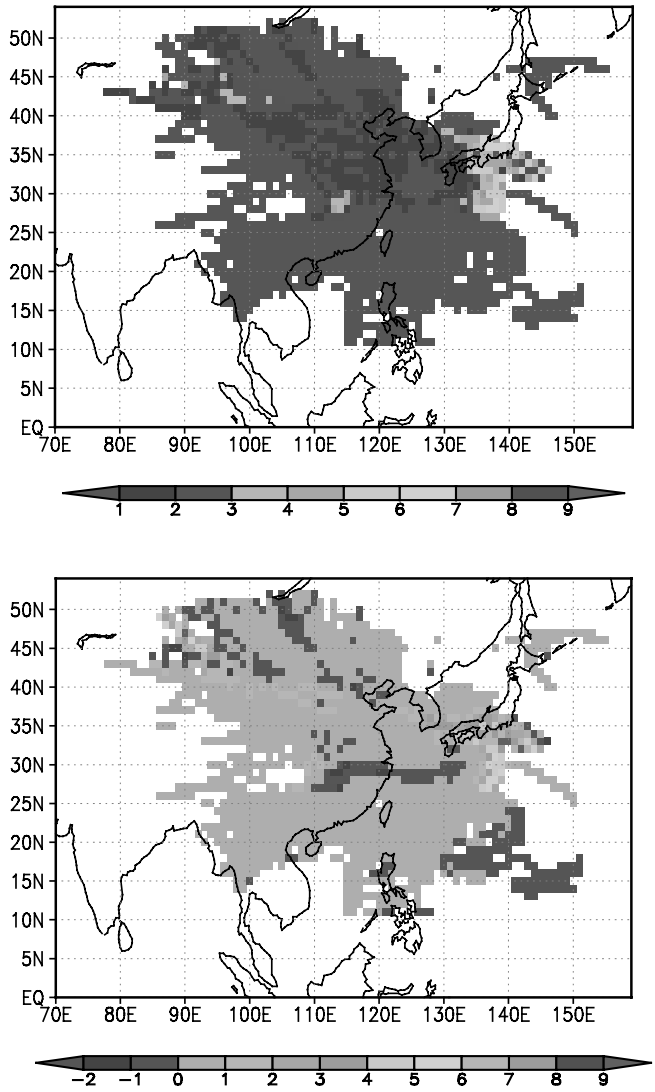

Figure 9. Mission-averaged average distribution of SO_2 below 2 km reconstructed using the aircraft observed values and back-trajectory analysis (upper), and the mean monthly bias between the reconstructed distribution based on the observations and the distribution reconstructed using the modeled values along the flight path (lower). All values are in ppbv. See color version of this figure at back of this issue.

[25] A doubling of the emissions moves the results in the right direction but does not eliminate the problems. Based on this analysis alone, the domestic sector would have to be increased by 3–5 times to reconcile the model results for CO with the observations. Clearly, the domestic sector emissions need further study.

[26] The results presented here are consistent with a recent global CO inverse modeling study by *Kasibhatla et al.* [2002]. Their inversion using surface observations of CO identified the need for significantly larger biomass (~100% higher), and biofuel and fossil fuel sources (~50% higher) of CO in Asia. Specifically their a priori estimate of CO emission in Asia was ~310 Tg-CO per year (210 Tg from fossil and biofuels and 100 Tg from biomass burning). Our base-line estimate of CO emissions from 2000 was 278 Tg-CO (211 Tg from fossil and biofuels, and 67 Tg from biomass burning). Their estimated emissions after inversion was ~350 Tg-CO from fossil and biofuels. Our value based on doubling of the domestic sector is ~380 Tg-CO from fossil and biofuel combustion. *Palmer et al.* [2003] performed an emissions inversion for CO using the TRACE-P aircraft observations. They recovered a posteriori emission value that was 30% higher for China than used in their forward analysis. A result that is also consistent with that derived here.

3.5. Megacity Analysis

[27] As shown in Figure 7 and discussed previously, the aircraft when flying in the Yellow Sea often measured very polluted air masses in plume-like structures at altitudes below ~2 km. It was also shown (Figure 11) that the model was able to locate the plumes at the right location but usually underpredicted the values. Examining ratios, instead of single species, helps to minimize effects that may be due to model resolution or other model errors associated with transport processes. For example, while the model may underpredict CO and propane in distinct plumes, the model may predict accurately the CO to propane ratio. In this section this hypothesis is tested and used to evaluate emission estimates from the largest Asian cities. Megacities were chosen for analysis as they have clear regional differences (as shown in Figure 3), their estimated emission and underlying activity data are better characterized, and they provide ambient concentrations that are well above background levels, making them easier to detect.

[28] The analysis of ratios was performed by first classifying the observations according to the megacity (as shown in Figure 3) and then calculating the ratios of selected species by regressing one species against the other. The analysis was further refined by regressing only data points of a specific age. In the case of emission estimates we assume that air masses younger than 1 day have the strongest emission signatures and the least uncertainty in the trajectories. This analysis was performed using the observational data and repeated for the modeled data. Sample results are shown in Figure 12. Shown in these plots are the observed and modeled values for all measurement points classified to be influenced by emissions from Shanghai within 24 hours of being sampled by the aircraft. The values were then analyzed as shown. All different combinations of pairs of species were plotted to determine their relationships. For example, observed C_3H_8 plotted against observed CO is shown in Figure 12. Also shown

Table 3. Observed and Calculated Values at the Lin'an Surface Site for March 2001

Species and Variables	Observed	Simulated
Mean CO (ppbv)	650	316
Mean SO_2 (ppbv)	16.5	5.2
Mean NO_y (ppbv)	13.2	4.1
Regression line of SO_2 versus CO[a]	$Y = 0.018 \times X + 4.8$	$Y = 0.0178 \times X - 0.3$
Regression line of NO_y versus CO	$Y = 0.021 \times X - 0.33$	$Y = 0.014 \times X - 0.4$
Regression line of SO_2 versus NO_y[a]	$Y = 0.9 \times X + 5.1$	$Y = 1.4 \times X - 0.7$

[a]Correlation coefficients r^2 are low (<0.2).

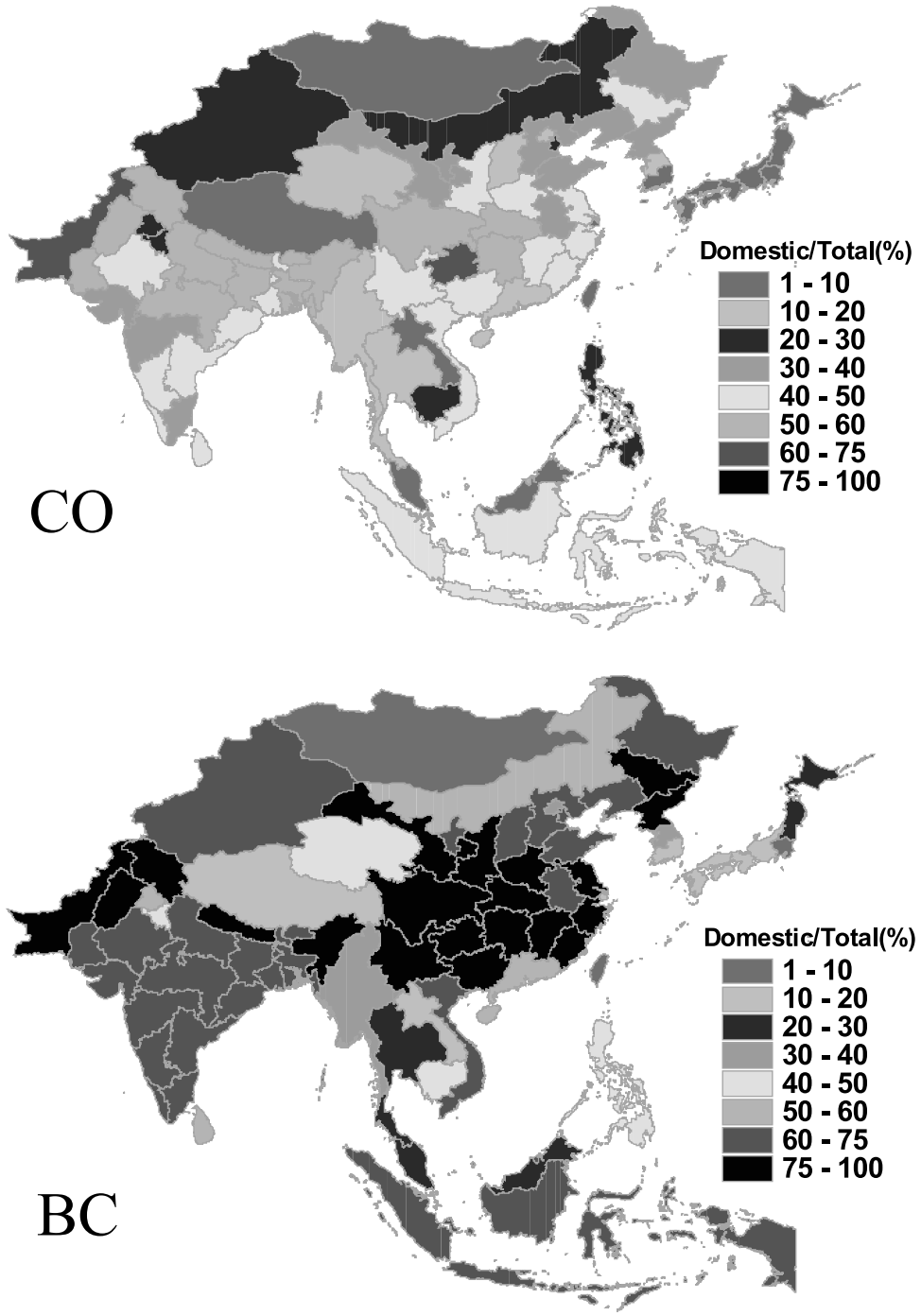

Figure 10. The regional distribution of the contribution of domestic sector emissions of CO and BC expressed as percentage of total emissions. See color version of this figure at back of this issue.

is the regression of modeled C_3H_8 with modeled CO. The slopes for observed and modeled values ($\Delta C_3H_8/\Delta CO$) along with r^2 values are presented in Tables 5 and 6 and are used in subsequent discussions. The idea is that if observed and modeled ratios are the same, then this implies that the emission ratios in the inventory are correct.

3.5.1. Shanghai

[29] A summary of calculated ratios for Shanghai is presented in Table 5, which is based on 80 km grid analysis. As discussed above, while both CO and propane are

Table 4. Domestic Sector Emissions by Fuel for 2000 (Annual Basis for the Domain of Figure 5)

Chemical Species	Domestic Sector			Percent of Domestic to Total Emisisons
	Fossil	Biofuel	Sum	
SO_2(Gg)	2549	1116	3665	11
NO_x(Gg)	795	1098	1893	7
CO(Gg)	8899	95721	104620	38
CO_2(Tg)	552	2132	2684	27
BC(Gg)	337	1294	1631	64
OC(Gg)	273	6473	6746	65

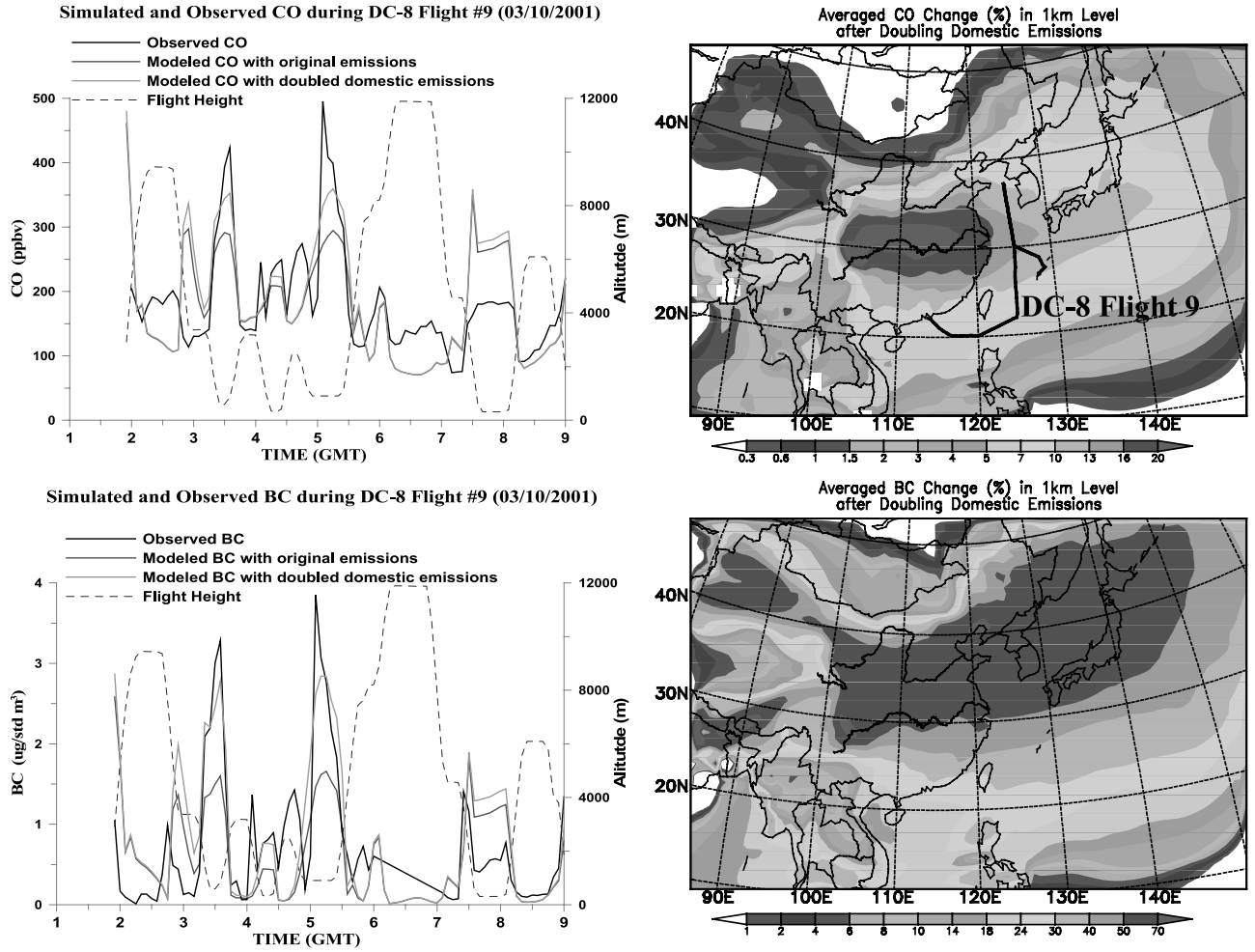

Figure 11. Results from sensitivity simulations using doubled domestic sector emissions. Monthly mean percentage change in near surface CO and BC levels for Asia (right) and along DC-8 flight 9. Flight track is shown. See color version of this figure at back of this issue.

systematically underpredicted at very high values, the calculated ratio is within ~10% of the observed ratio. Many of the model derived ratios fall within ~25% of those observed, and all fall within a factor of 2.5. The $\Delta HCHO/\Delta CO$ ratio is influenced more by the photochemical processes than by the ratio in the primary emissions. The coefficients of determination (i.e., r^2) are also shown. In most cases the model-based analysis show higher r^2 values than the observation-based analysis, reflecting that collectively the model system (emissions, resolution, transport, chemistry, removal) does not represent all of the variability in the atmosphere and the fact that the classification scheme is based on the modeled winds, which are the same winds used in the forward model simulations.

[30] To explore the sensitivity of the analysis to some of the key factors, the analysis was repeated using the results from a fine-grid STEM-2K1 calculation (i.e., 16 km grids). In general the results differed by at most ±25% (e.g., the 16 km value of $\Delta SO_2/\Delta CO$ for the Shanghai plumes was 0.015 (r^2 = 0.52) for the observation-based analysis and 0.017 (r^2 = 0.40) for the model-based analysis). The results were also repeated for different air mass ages. For ratios of species that are not very reactive (e.g., $\Delta BC/\Delta CO$) the results were insensitive (less than 5% difference) to air mass age.

[31] The emission ratios estimated from the inventory for Shanghai are also shown in Table 5. For the low reactive species, the ratios are consistent with those derived from the observations (e.g., $\Delta BC/\Delta CO$, $\Delta C_2H_6/\Delta CO$, $\Delta C_2H_2/\Delta CO$). Since there are many sources of uncertainty in the model that influence the relationship between emissions and subsequent trace gas distributions, disagreement does not automatically imply inaccuracies in emissions. For example, ratios will change over time if the chemical reaction rates of the species are different. To illustrate, for the Shanghai plumes, both the observation-based and model-based analysis produce a value of Δethane/Δethene of ~1–1.3, while the emission estimate yields a value of 0.33. Ethene reacts faster than ethane with OH, and by this processes values of Δethane/Δethene increase with travel time (consistent with the analysis). BC and CO are relatively long-lived species from chemical and removal perspectives, and their analyzed ratios are close to the emission ratio.

[32] The analysis was also repeated for the double-domestic sector emissions scenario. Selected results for Shanghai are shown in Table 5. In general the regressions became stronger in the model and the results closer to the observations. The most important results are for the $\Delta C_2H_2/\Delta CO$ and $\Delta SO_x/\Delta C_2H_2$ values, which show that

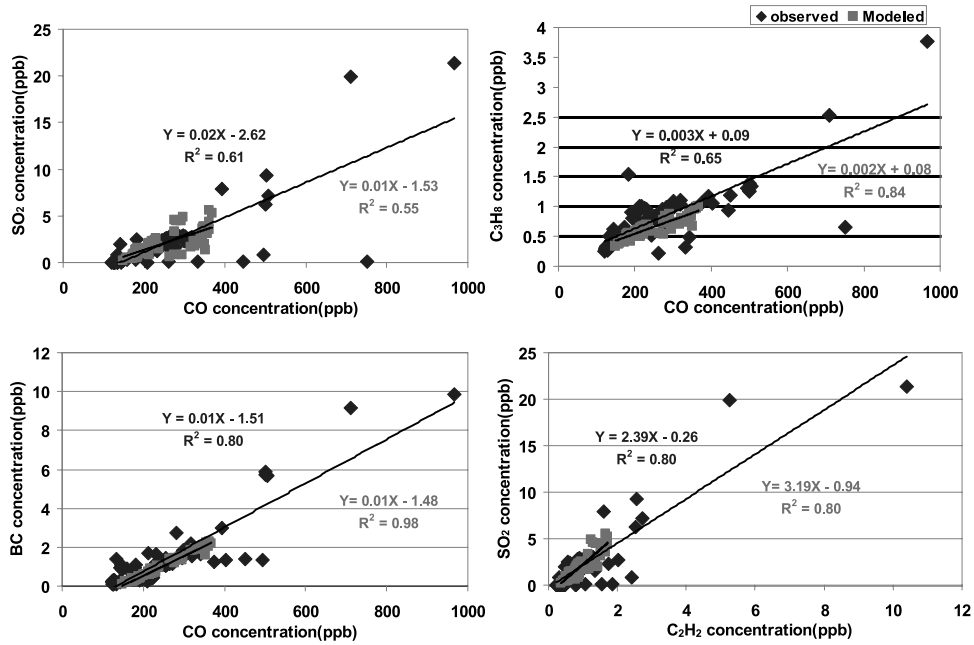

Figure 12. Examples of regression analysis of various species using aircraft observations identified to have encountered Shanghai air masses less than 1 day old (blue). Also shown are values estimated using modeled values for these same data points (pink). See color version of this figure at back of this issue.

the domestic sector preferentially increases ethyne relative to CO and to SO_x, producing results much closer to the observations.

3.5.2. All Megacities

[33] A summary of estimated ratios for all cities with more than 25 data points is presented in Table 6, and the emission ratios are presented in Table 7. The results for these cities are similar to those discussed for Shanghai, so a city-by-city discussion is not presented. Comparing measured and modeled ratios, some clear trends are observed that reflect regional differences and that are consistent with the estimated emissions. One example is the $\Delta BC/\Delta CO$ values. The highest values are retrieved for Tokyo (0.017) and Seoul (0.014), with the Chinese cities having lower values (0.011). These values are consistent with the estimated BC and CO emissions. In addition, the propane/benzene and nitrogen-oxides/sulfur-oxides values are much higher for Seoul, Pusan, and Tokyo than in the Chinese cities, while the opposite is true for the sulfur-oxides/ethyne values. These trends reflect lower sulfur dioxide and higher nitrogen oxide emissions in Seoul, Pusan, and Tokyo, associated with a larger role of the transportation sector and a lesser dependence on coal in these cities.

[34] There is also a general consistency between the observed and modeled ratios for $\Delta BC/\Delta CO$, $\Delta SO_x/\Delta C_2H_2$, and $\Delta C_2H_6/\Delta C_2H_4$. Furthermore, the north-central China cities of Tianjin, Beijing, and Qingdao have ratios that are very similar to each other but different than those for Shanghai. For all of the ratios involving CO in the denominator, the model-derived values are 2–3 times larger than the observation-derived values for these north-central Chinese cities. This is not the case for ratios involving ethyne. For example, there is good agreement between the observed and modeled $\Delta SO_x/\Delta C_2H_2$ values for this region.

Table 5. Estimated Ratios of Selected Species for Data Points Identified as Shanghai Plumes for Air Mass Ages Less Than 1 Day Based on the 80 km Grid Analysis[a]

$\Delta X/\Delta Y$	Observed	Modeled	2 × Domestic	Emissions (Base Case)
$\Delta BC/\Delta CO$	0.011 (0.80)[b]	0.010 (0.98)	0.012 (0.99)	0.008
$\Delta BC/\Delta SO_2$	0.48 (0.90)	0.38 (0.52)	0.55 (0.61)	0.07
$\Delta HCHO/\Delta CO$	0.011 (0.70)	0.006 (0.80)	0.006 (0.85)	0.002
$\Delta C_2H_6/\Delta CO$	0.004 (0.71)	0.006 (0.86)	0.007 (0.92)	0.004
$\Delta C_2H_6/\Delta C_2H_2$	0.39 (0.62)	1.14 (0.96)	1.03 (0.98)	0.66
$\Delta C_2H_6/\Delta C_2H_4$	0.96 (0.59)	1.32 (0.53)	1.22 (0.73)	0.33
$\Delta SO_x/\Delta C_2H_2$	3.71 (0.77)	5.69 (0.76)	3.64 (0.76)	17.6
$\Delta NO_y/\Delta SO_x$	0.35 (0.92)	0.88 (0.91)	0.85 (0.90)	1.0
$\Delta C_3H_8/\Delta CO$	0.0027 (0.65)	0.0023 (0.84)	0.0031 (0.89)	0.005
$\Delta C_2H_2/\Delta CO$	0.0076 (0.76)	0.0051 (0.88)	0.0067 (0.92)	0.0063
$\Delta C_2H_6/\Delta C_3H_8$	1.19 (0.85)	2.51 (0.98)	2.23 (0.98)	0.81
$\Delta SO_2/\Delta CO$	0.0187 (0.61)	0.0144 (0.55)	0.0129 (0.60)	0.11

[a]Results determined from calculations using base emissions and for doubled domestic sector emissions are shown. Ratios determined from the base-emissions are also presented.

[b]Numbers in parenthesis represent r^2 values.

Table 6. Calculated Ratios of Selected Species for Various Megacities for Air Mass Ages Less Than 1 Day[a]

	Seoul-Inchon		Pusan		Tokyo		Shanghai		Hong Kong		Tianjin		Beijing		Qingdao	
Species	Slope	r^2	Slope	r^2	Slope	r^2	Slope	r^2	Slope	r^2	Slope	r^2	Slope	r^2	Slope	r^2
HCHO/CO O							0.011	(0.70)			0.016	(0.30)				
HCHO/CO M	0.005	(0.69)	0.009	(0.63)	0.005	(0.61)	0.006	(0.804)	0.001	(0.23)	0.008	(0.92)	0.011	(0.77)	0.010	(0.92)
HCHO/C_2H_2 O							0.909	(0.56)			5.042	(0.49)				
HCHO/C_2H_2 M	0.47	(0.31)	0.38	(0.024)	0.66	(0.34)	1.13	(0.92)	0.69	(0.61)	1.13	(0.92)	1.38	(0.67)	1.20	(0.85)
C_2H_6/CO O	0.007	(0.76)	0.007	(0.77)	0.004	(0.70)	0.004	(0.71)	0.005	(0.54)	0.004	(0.42)	0.005	(0.61)	0.004	(0.32)
C_2H_6/CO M	0.006	(0.59)	−0.001	(0.006)	0.007	(0.88)	0.006	(0.86)	0.004	(0.52)	0.008	(0.96)	0.009	(0.86)	0.009	(0.93)
C_2H_6/C_2H_4 O	0.96	(0.49)	2.31	(0.69)	0.54	(0.77)	0.96	(0.59)	1.45	(0.43)	3.62	(0.77)	4.86	(0.86)	1.84	(0.21)
C_2H_6/C_2H_4 M	1.18	(0.58)	1.48	(0.53)	1.29	(0.64)	1.32	(0.54)	2.34	(0.57)	2.12	(0.91)	1.65	(0.92)	1.52	(0.69)
C_2H_6/C_2H_2 O	1.69	(0.88)	1.73	(0.86)	1.20	(0.89)	0.39	(0.62)	1.12	(0.87)	2.092	(0.71)	2.24	(0.81)	1.83	(0.62)
C_2H_6/C_2H_2 M	1.17	(0.94)	1.40	(0.79)	1.41	(0.99)	1.14	(0.96)	1.64	(0.92)	1.19	(0.98)	1.27	(0.92)	1.25	(0.97)
C_3H_8/CO O	0.007	(0.82)	0.004	(0.82)	0.007	(0.85)	0.003	(0.65)	0.002	(0.26)	0.002	(0.29)	0.002	(0.48)	0.002	(0.22)
C_3H_8/CO M	0.003	(0.51)	−0.0005	(0.012)	0.004	(0.84)	0.002	(0.84)	0.002	(0.55)	0.003	(0.91)	0.005	(0.88)	0.004	(0.94)
C_3H_8/Benzene O	4.30	(0.89)	3.31	(0.90)	3.78	(0.90)	1.08	(0.81)	2.43	(0.76)	2.45	(0.57)	2.52	(0.69)	1.81	(0.39)
C_3H_8/Benzene M																
BC/SO_2 O	3.66	(0.57)			2.39	(0.30)	0.48	(0.90)			0.28	(0.62)			0.39	(0.91)
BC/SO_2 M	0.19	(0.51)	0.067	(0.04)	−0.003	(0.005)	0.38	(0.52)	0.29	(0.082)	0.22	(0.92)	0.13	(0.97)	0.15	(0.82)
BC/CO O	0.014	(0.96)			0.017	(0.84)	0.011	(0.80)	0.011	(0.19)	0.011	(0.94)			0.011	(0.94)
BC/CO M	0.010	(0.96)	0.011	(0.92)	0.008	(0.87)	0.010	(0.98)	0.007	(0.96)	0.010	(0.94)	0.007	(0.81)	0.009	(0.94)
NO_y/CO O	0.003	(0.038)	0.016	(0.70)	0.040	(0.29)	0.011	(0.62)	0.0001	(0.0005)	0.013	(0.51)	0.018	(0.63)	0.015	(0.48)
NO_y/CO M	0.070	(0.64)	0.053	(0.50)	0.074	(0.73)	0.027	(0.66)	0.004	(0.10)	0.043	(0.97)	0.051	(0.92)	0.050	(0.98)
NO_Y/SO_x O	0.76	(0.51)	0.83	(0.66)	−0.18	(0.021)	0.35	(0.92)	0.19	(0.19)	0.43	(0.66)	0.46	(0.64)	0.45	(0.56)
NO_Y/SO_x M	1.35	(0.77)	0.70	(0.31)	−0.093	(0.046)	0.88	(0.91)	0.90	(0.78)	0.57	(0.98)	0.67	(0.97)	0.65	(0.98)
SO_x/CO O	0.008	(0.28)	0.012	(0.43)	−0.012	(0.040)	0.028	(0.59)	0.003	(0.113)	0.032	(0.89)	0.037	(0.96)	0.035	(0.89)
SO_x/CO M	0.053	(0.88)	0.019	(0.096)	−0.037	(0.034)	0.026	(0.51)	0.003	(0.08)	0.075	(0.97)	0.073	(0.87)	0.075	(0.96)
SO_x/C_2H_2 O	4.41	(0.85)	2.82	(0.46)	−2.38	(0.023)	3.71	(0.77)	0.30	(0.053)	10.66	(0.61)	12.75	(0.68)	9.19	(0.50)
SO_x/C_2H_2 M					−15.2	(0.16)	5.70	(0.76)	2.63	(0.57)	10.78	(0.95)	10.03	(0.84)	9.44	(0.92)
C_2H_2/CO O	0.004	(0.95)	0.004	(0.92)	0.004	(0.88)	0.008	(0.76)	0.005	(0.73)	0.002	(0.68)	0.002	(0.78)	0.002	(0.73)
C_2H_2/CO M	0.006	(0.78)	0.001	(0.008)	0.005	(0.87)	0.005	(0.88)	0.002	(0.53)	0.007	(0.98)	0.007	(0.99)	0.008	(0.98)
C_2H_6/C_3H_8 O	0.89	(0.77)	1.59	(0.89)	0.59	(0.86)	1.19	(0.85)	1.59	(0.88)	1.81	(0.97)	1.88	(0.98)	1.92	(0.94)
C_2H_6/C_3H_8 M	1.74	(0.91)	1.51	(0.84)	1.80	(0.90)	2.51	(0.98)	2.22	(0.98)	2.39	(0.98)	1.95	(0.99)	2.17	(0.99)

[a]O = Observed; M = Modeled.

[35] This analysis shows interesting features regarding sulfur emissions around Tokyo. As shown in the Table 6, all the analyzed ratios involving sulfur (observed and model) for Tokyo show negative slopes and low correlations. This is due to the large impact of sulfur emissions from the Miyakejima volcano. These emissions do not contain NMHC or NO_x or CO. This illustrates how this analysis can help identify source types.

4. Summary

[36] In this paper we explored various ways in which measurements made during the NASA TRACE-P experiment could be used in conjunction with regional modeling analysis to evaluate emission estimates for Asia. The first evaluation involved comparisons between the modeled values and the aircraft observations. Based on this analysis we conclude that the inventory performs well for the light alkanes, CO, ethyne, SO_2, and NO_x. Furthermore, the model was shown to have skill in predicting important photochemical species such as O_3, HCHO, OH, HO_2, and HNO_3. These results indicate that the emissions inventories are of sufficient quality to support modeling studies of photochemistry. These are important findings in light of the fact that emission estimates for many species (such as speciated NMHCs and BC) for this region have only recently been estimated and are highly uncertain.

Table 7. Ratios (Molar) of Various Species Determined From the Emission Estimates for the Cities Analyzed

	Seoul-Inchon	Pusan	Tokyo	Shanghai	Hong Kong	Tianjin	Beijing	Qingdao
HCHO/CO	0.0122	0.0029	0.0037	0.0023	0.0097	0.0024	0.0024	0.0026
HCHO/C2H2	1.49	0.94	1.12	0.36	1.48	0.38	0.35	0.28
C2H6/CO	0.009	0.003	0.005	0.004	0.012	0.005	0.004	0.005
C2H6/C2H4	0.50	0.42	0.45	0.33	0.54	0.64	0.48	0.51
C2H6/C2H2	1.13	0.98	1.63	0.66	1.76	0.79	0.59	0.53
C3H8/CO	0.010	0.003	0.005	0.005	0.011	0.006	0.005	0.006
C3H8/benzene	5.21	3.06	5.90	3.98	5.25	6.21	5.21	6.43
BC/SO2	0.13	0.23	0.44	0.07	0.05	0.11	0.11	0.07
BC/CO	0.03	0.01	0.02	0.01	0.01	0.01	0.01	0.01
NOy/CO	0.42	0.19	0.21	0.11	0.72	0.10	0.05	0.11
NOy/SOx	2.0	3.0	5.3	1.0	2.7	0.9	0.9	0.6
SOx/CO	0.21	0.06	0.04	0.11	0.27	0.11	0.06	0.20
SOx/C2H2	25.1	20.2	12.1	17.6	40.5	17.1	8.8	22.0
C2H2/CO	0.0082	0.0031	0.0033	0.0063	0.0066	0.0064	0.0069	0.0092
C2H6/C3H8	0.91	1.18	0.97	0.81	1.05	0.89	0.82	0.81

[37] We further explored how the observations could be classified using back-trajectory analysis. Using a classification of the measurements built upon trajectory analysis, we compared observed species distributions and ratios of species to those modeled and to ratios estimated from the emissions inventory. It was shown that this technique could reconstruct a spatial distribution of propane/benzene that looks remarkably similar to that calculated from the emissions inventory. This analysis works best using ratios of species with similar chemical reaction loss rates with respect to OH and that have some degree of spatial homogeneity within regions, as mixing effects as well as differences in reaction rates result in changes in the ratio along the trajectory.

[38] A major discrepancy between modeled and observed behavior was found over the Yellow Sea, where modeled values were systematically underpredicted. The integrated analysis suggests that this may be related to an underestimation of emissions from the domestic sector. A sensitivity calculation using doubled domestic sector emissions showed that emissions from this sector have a large influence on trace species concentrations over central China and in the Yellow Sea. Based on this analysis alone, the domestic sector would have to be increased by 3–5 times to reconcile the model results for CO with the observations. This result is consistent with recent results from formal inversions using global models. Clearly, the domestic sector emissions need further study.

[39] The emissions were further tested by comparing observed and measured species ratios in identified megacity plumes. Many of the model-derived ratios (e.g., $\Delta BC/\Delta CO$, $\Delta SO_x/\Delta C_2H_2$) were shown to fall within ~25% of those observed, and only $\Delta C_2H_6/\Delta C_2H_2$, $\Delta HCHO/\Delta CO$, and $\Delta NO_x/\Delta CO$ differed by more than a factor of 2. The analysis of the observations for different cities detected regional differences, which reflect the lower sulfur dioxide and higher nitrogen oxide emissions in Seoul, Pusan, and Tokyo, associated with a larger role of the transportation sector and a lesser dependence on coal in these cities. Furthermore, the north-central China cities of Tianjin, Beijing, and Qingdao were found to have ratios that were very similar to each other, but different than those for Shanghai. The analysis was also able to detect the presence of a large sulfur source that did not emit CO, NO_x, or NMHC. This was obviously due to emissions from the Miyakejima volcano but demonstrates the potential to detect unknown sources.

[40] The results presented illustrate how measurements obtained during the NASA TRACE-P experiment, when integrated with modeling analysis, provide a means to evaluate the quality of emission estimates. Clearly, there is a wealth of information contained in such analysis, and more work is needed along this line of merging emissions with observation-based and model-based analysis. In the future it is recommended that emissions testing play an even larger role in large-scale experiments. Furthermore, the above analysis has focused largely on the use of trace gas emissions and measurements. What is needed to make this analysis more powerful is to extend this information using aerosol composition. Techniques, such as single particle analysis, are well suited for this use as they can provide more specific source profiles (e.g., distinguish coal from biofuel, and anthropogenic dust-fly ash and cement manufacturing from wind blow soils). In addition it is possible to use the observation-based analysis to improve emission estimates. The observed ratios for specific megacities and regions could be used in a regional inversion methodology to revise the bottom-up emission inventory. This methodology could also be used directly to construct a regional inventory. We are presently exploring these techniques to create a mercury emissions inventory using observations from the Ace-Asia experiment.

[41] **Acknowledgments.** This work was supported in part by grants from the NASA GTE and ACMAP programs and the NSF Atmospheric Chemistry Program. This work (I. Uno) was also partly supported by Research and Development Applying Advanced Computational Science and Technology (ACT-JST) and CREST of the Japan Science and Technology Corporation. Tao Wang acknowledges financial support from the Research Grants Council of the Hong Kong Special Administrative Region (Project PolyU 5063/01E).

References

Carmichael, G. R., et al., Regional-scale chemical transport modeling in support of intensive field experiments: Overview and analysis of the TRACE-P observations, *J. Geophys. Res.*, *108*(D21), 8823, doi:10.1029/2002JD003117, in press, 2003.

Carter, W., Documentation of the SAPRC-99 chemical mechanism for voc reactivity assessment, Final Report to California Air Resources Board, *contract 92-329*, Univ. of Calif., Riverside, Riverside, Calif., 2000.

Kasibhatla, P., A. Arellano, J. Logan, and P. Palmer, Top-down estimate of a large source of atmospheric carbon monoxide associated with fuel combustion in Asia, *Geophys. Res. Lett.*, *29*(19), 1900, doi:10.1029/2002GL015581, 2002.

Kiley, C. M., et al., An intercomparison and validation of aircraft-derived and simulated CO from seven chemical transport models during the TRACE-P experiment, *J. Geophys. Res.*, *108*(D21), 8819, doi:10.1029/2002JD003089, in press, 2003.

Madronich, S., and S. Flocke, The role of solar radiation in atmospheric chemistry, in *Handbook of Environmental Chemistry*, edited by P. Boule, pp. 1–26, Springer-Verlag, New York, 1999.

National Research Council (NRC), *Rethinking the Ozone Problem in Urban and Regional Pollution*, 489 pp., National Academy Press, Washington, D. C., 1991.

Palmer, P., D. J. Jacob, D. B. A. Jones, C. L. Heald, R. M. Yantosca, J. Logan, G. Sacshe, and D. Streets, Inverting for emissions of carbon monoxide from Asia using aircraft observations over the western Pacific, *J. Geophys. Res.*, *108*(D21), 8828, doi:10.1029/2003JD003397, in press, 2003.

Pielke, R. A., et al., A comprehensive meteorological modeling system–RAMS, *Meteorol. Atmos. Phys.*, *49*, 69–91, 1992.

Streets, D. G., et al., An inventory of gaseous and primary aerosol emissions in Asia in the year 2000, *J. Geophys. Res.*, *108*(D21), 8809, doi:10.1029/2002JD003093, in press, 2003a.

Streets, D., K. F. Yarber, J.-H. Woo, and G. R. Carmichael, Biomass burning in Asia: Annual and seasonal estimates and atmospheric emissions, *Global Biogeochem. Cycles*, *17*, doi:10.1029/2003GB002040, in press, 2003b.

Tang, Y., et al., Impacts of aerosols and clouds on photolysis frequencies and photochemistry during TRACE-P: 2. Three-dimensional study using a regional chemical transport model, *J. Geophys. Res.*, *108*(D21), 8822, doi:10.1029/2002JD003100, in press, 2003a.

Tang, Y., et al., Influences of biomass burning during TRACE-P experiment identified by the regional chemical transport model, *J. Geophys. Res.*, *108*(D21), 8824, doi:10.1029/2002JD003110, in press, 2003b.

Uno, I., et al., Regional chemical weather forecasting using CFORS: Analysis of surface observation at Japanese Island Station during the ACE-Asia experiment, *J. Geophys. Res.*, *108*(D23), 8668, doi:10.1029/2002JD002845, 2002.

Verwer, J. G., E. J. Spee, J. G. Blom, and W. H. Hundsdorfer, A second order Rosenbrock method applied to photochemical dispersion problems, *SIAM J. Sci. Comput.*, *20*(4), 14,456–14,480, 1999.

Wang, T., V. T. F. Cheung, M. Anson, and Y. S. Li, Ozone and related gaseous pollutants in the boundary layer of eastern China: Overview of the recent measurements at a rural site, *Geophys. Res. Lett.*, *28*, 2372–2376, 2001.

Wang, T., T. F. Cheung, Y. S. Li, X. M. Yu, and D. R. Blake, Emission characteristics of CO, NO_x, SO_2 and indications of biomass burning observed at a rural site in eastern China, *J. Geophys. Res.*, *107*(D12), 4157, doi:10.1029/2001JD000724, 2002.

Woo, J.-H., D. G. Streets, G. R. Carmichael, Y. Tang, B.-I. Yoo, W.-C. Lee, N. Thongboonchoo, S. Pinnock, G. Kurata, and I. Uno, Biomass and Biofuel Emissions and Their Impact on Trace Gas Distributions in Asia during the TRACE-P Experiment, *J. Geophys. Res.*, *108*(D21), 8812, doi:10.1029/2002JD003200, in press, 2003.

Yoshino, A., H. Nagai, N. Umeyama, and M. Chino, Real-time simulation and analysis on long range atmospheric dispersion of volcanic gases discharged from the Miyajima Island, *J. Jpn. Soc. Atmos. Environ.*, *37*, 23–34, 2002.

E. Atlas, National Center for Atmospheric Research, Boulder, CO 80305, USA. (atlas@ucar.edu)

M. A. Avery and G. W. Sachse, NASA Langley Research Center, Hampton, VA 23681, USA. (m.a.avery@larc.nasa.gov; g.w.sachse@larc.nasa.gov)

A. Bandy and D. Thornton, Chemistry Department, Drexel University, Philadelphia, PA, USA. (bandyar@drexel.edu; dct@drexel.edu)

D. R. Blake, Department of Chemistry, University of California, Irvine, Irvine, CA 92697, USA. (drblake@uci.edu)

G. R. Carmichael, S. Guttikunda, Y. Tang, N. Thongboonchoo, and J.-H. Woo, Center for Global and Regional Environmental Research, University of Iowa, Iowa City, IA 52242, USA. (gcarmich@engineering.uiowa.edu; sguttiku@cgrer.uiowa.edu; ytang@cgrer.uiowa.edu; nthongbo@cgrer.uiowa.edu; woojh21@cgrer.uiowa.edu)

A. D. Clarke, School of Ocean and Earth Science and Technology, University of Hawaii, Honolulu, HI 96822, USA. (tclarke@soest.hawaii.edu)

A. Fried and A. White, Department of Chemical Engineering, University of California, Davis, Davis, CA, USA. (fried@ucar.edu; adwhite@ucdavis.edu)

Y. Kondo, Research Center for Advanced Science and Technology, University of Tokyo, Meguro-ku, Tokyo 153-8904, Japan. (kondo@atmos.rcast.u-tokyo.ac.jp)

G. Kurata, Department of Ecological Engineering, Toyohashi University of Technology, Toyohashi, Aichi 441-8580, Japan. (kurata@eco.tut.ac.jp)

B. Potter, Department of Chemistry, University of Tulsa, Tulsa, OK 74101, USA. (william-potter@utulsa.edu)

S. T. Sandholm, School of Earth and Atmospheric Sciences, Georgia Institute of Technology, Atlanta, GA 30332, USA. (scott.sandholm@eas.gatech.edu)

D. G. Streets, Decision and Information Sciences Division, Argonne National Laboratory, Argonne, IL 60439, USA. (dstreets@anl.gov)

R. W. Talbot, Institute for the Study of Earth, Oceans, and Space, University of New Hampshire, Durham, NH 03824, USA. (robert.talbot@unh.edu)

I. Uno, Research Institute for Applied Mechanics, Kyushu University, Fukuoka 816-8580, Japan. (iuno@riam.kyushu-u.ac.jp)

T. Wang, Department of Civil and Structural Engineering, Hong Kong Polytechnic University, Hong Kong, China. (cetwang@polyu.edu.hk)

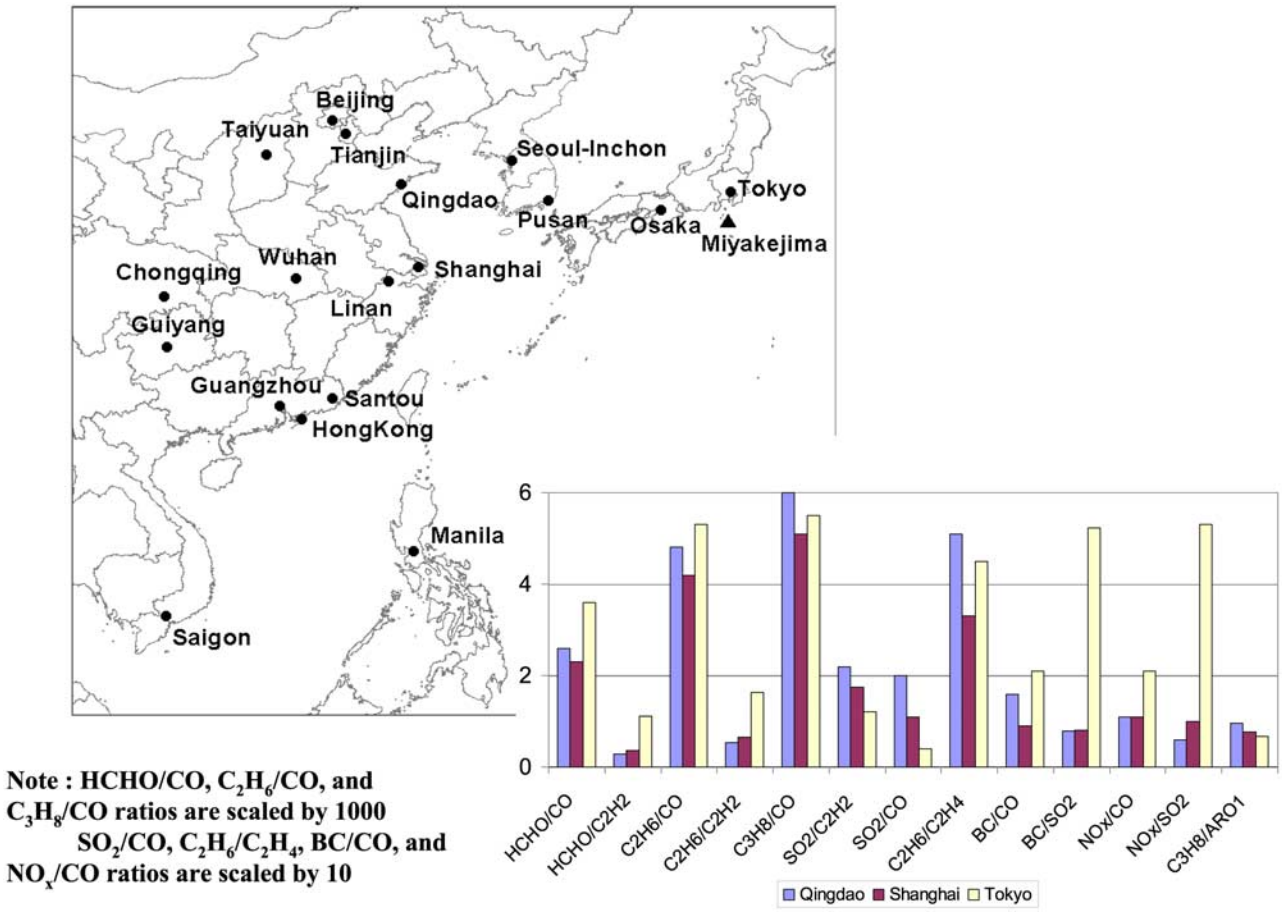

Figure 1. Domain used in the emissions and modeling analysis. Also shown are the locations of the megacities and the Miyakejima volcano. Emission ratios (molar) for a variety of species used in the analysis for Shanghai, Tokyo and Qingdao are also shown.

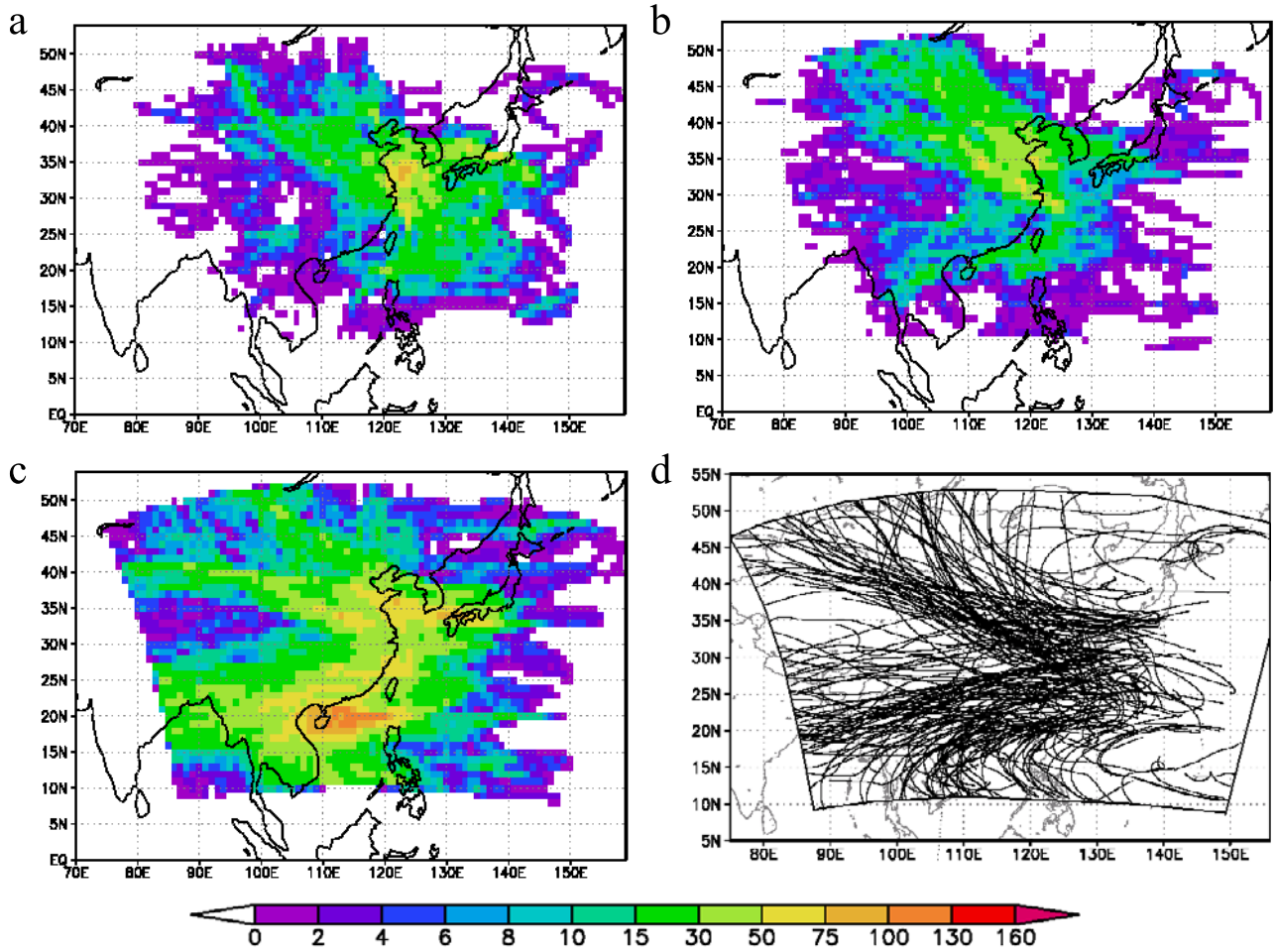

Figure 2. Trajectory statistics for 5-day back-trajectories calculated for every 5-min flight segment along the 12 DC-8 (4 March to 1 April) and 12 P-3B (4 March to 2 April) flights. Shown are the number of times the back-trajectories passed over each 1° × 1° grid cells below 1.5 km (a), between 1.5 and 3 km (b), over 3 km (c). Sample trajectories are shown in Figure 2d, which include ~2200 trajectories.

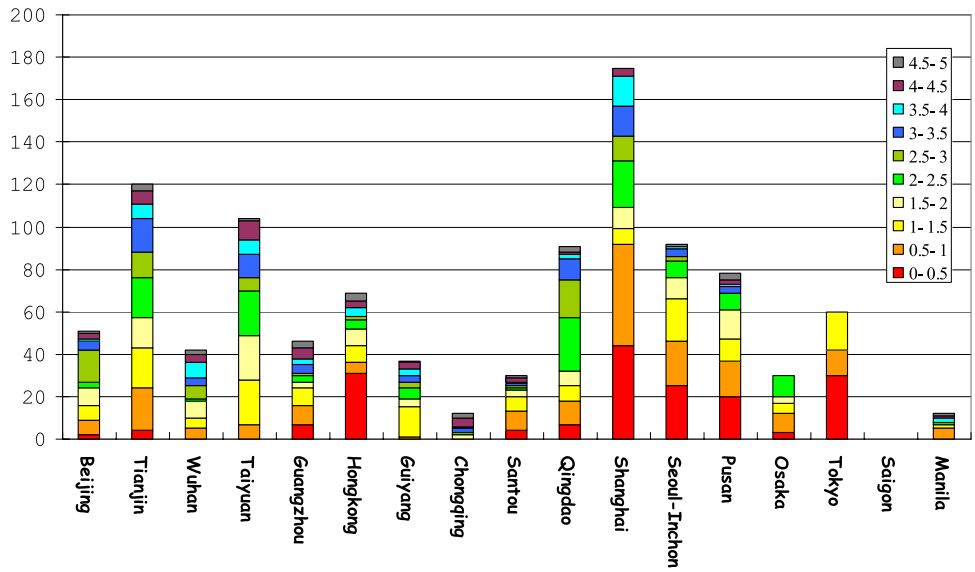

Figure 3. Trajectory statistics for 5-day back-trajectories calculated for every 5-min flight segment along the 12 DC-8 and 12 P-3B flights. Shown are the number of times the back-trajectories passed over selected megacities at altitudes below 2 km, classified by the age of the air mass (days). Emission ratios (molar) for a variety of species used in the analysis for Shanghai, Tokyo, and Qingdao are also shown.

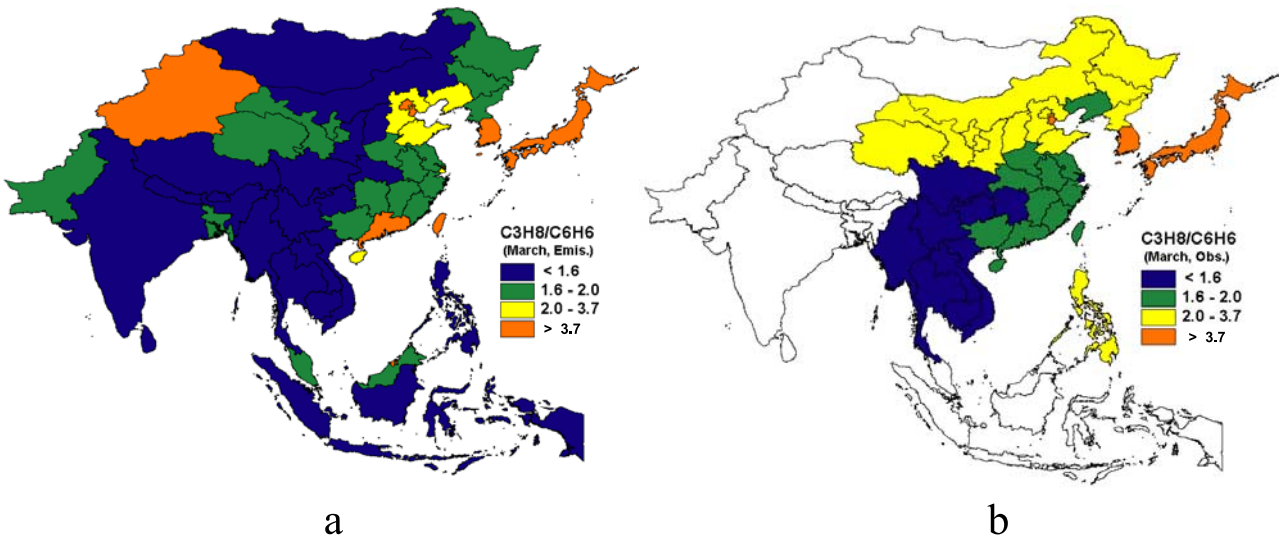

Figure 4. The regional distribution of propane to benzene ratio (molar) determined from the emissions inventory (a) and by back-trajectory analysis using the ratios observed onboard the aircrafts in all flights (b).

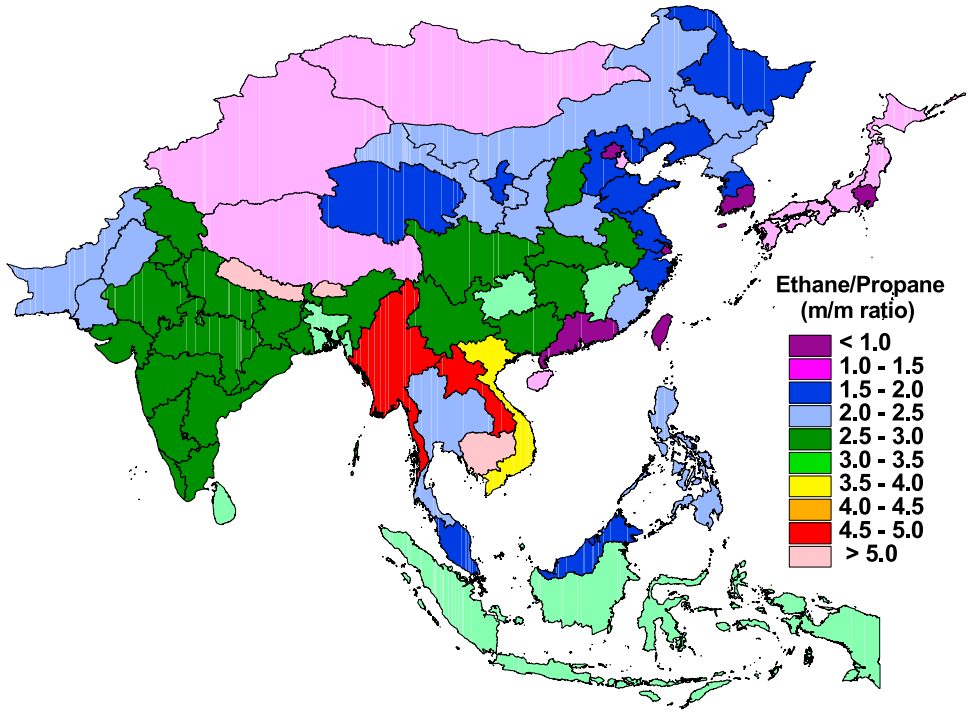

Figure 5. The regional distribution of ethane to propane ratios (molar) determined from the emissions inventory.

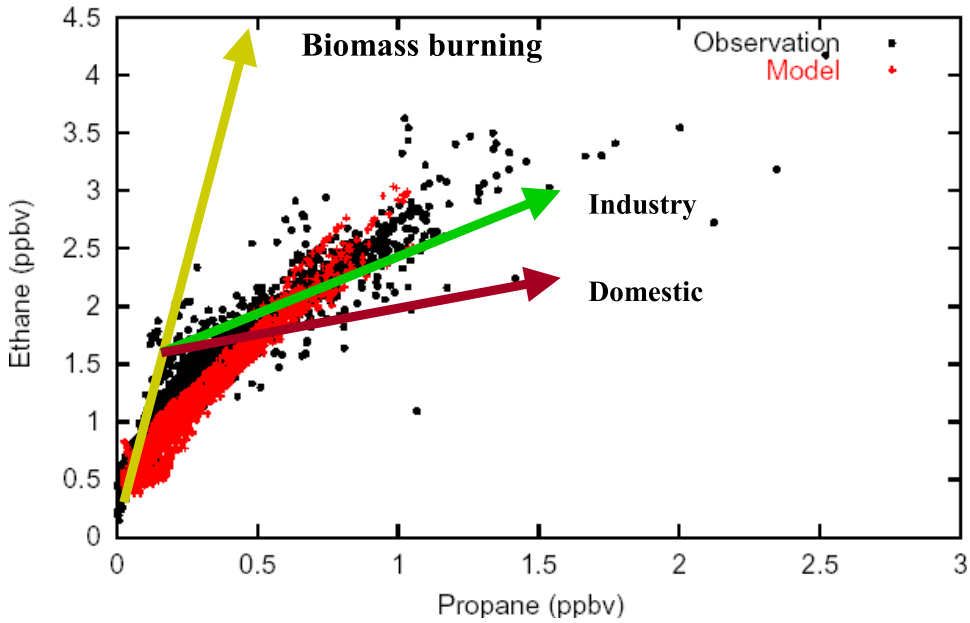

Figure 6. Observed and modeled relation between ethane to propane for the 5-min segments of the P-3B and DC-8 flights. Colored arrows show emission ratio for various sources categories.

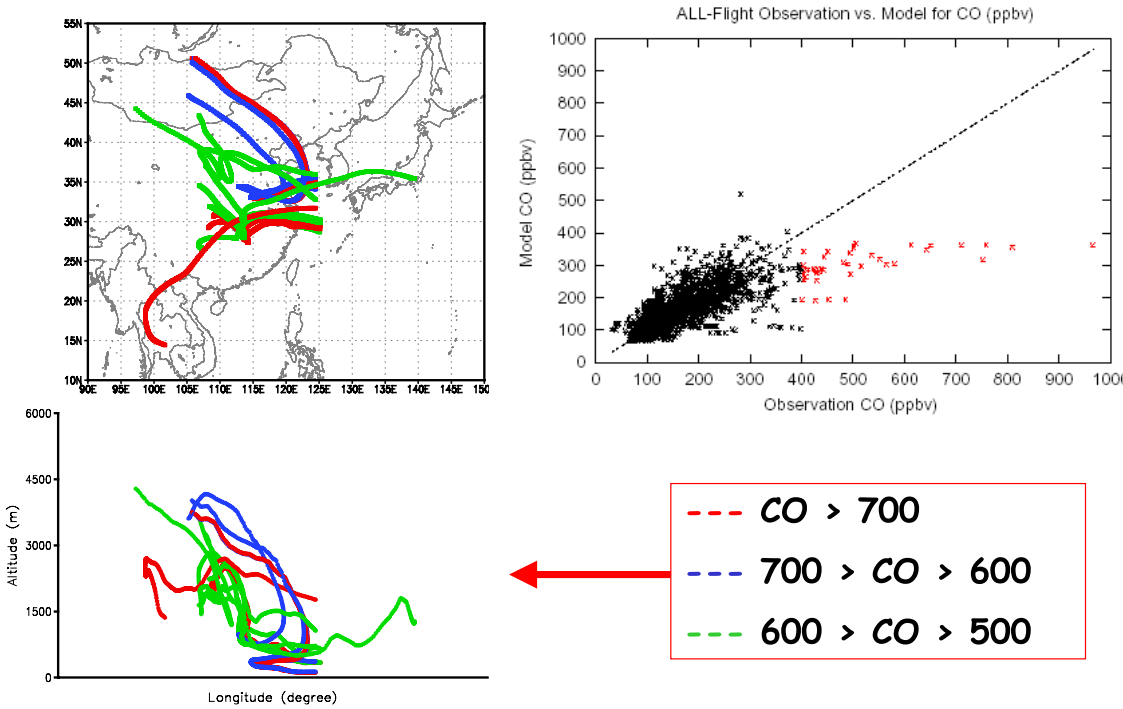

Figure 7. Modeled and observed CO for the DC-8 and P-3B flights (5-min merged data set). The red points indicate data points for which back-trajectories were calculated. The trajectories for the points with CO > 500 ppb are shown (left) and color-coded according to measured CO values.

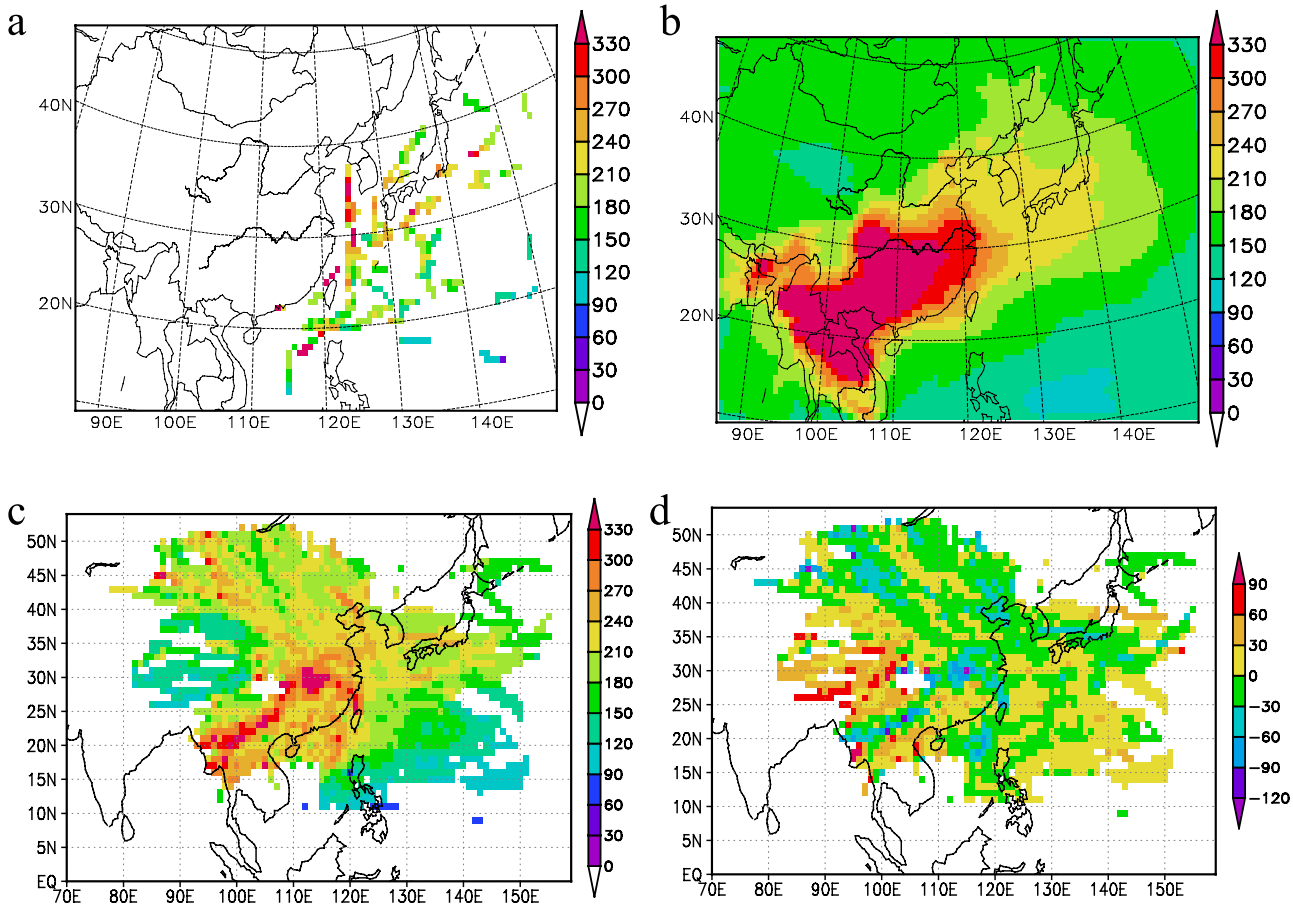

Figure 8. Mission-averaged distributions of CO. Averaged values of aircraft observation for altitudes below 2 km (a); model calculated values for all day-time points in the month of March for altitudes below 2 km (b); average distribution below 2 km reconstructed using the aircraft observed values and back-trajectory analysis (c); and mean monthly bias below 2 km between the reconstructed distribution based on the observations and the distribution reconstructed using the modeled values along the flight path (d). All values are in ppbv.

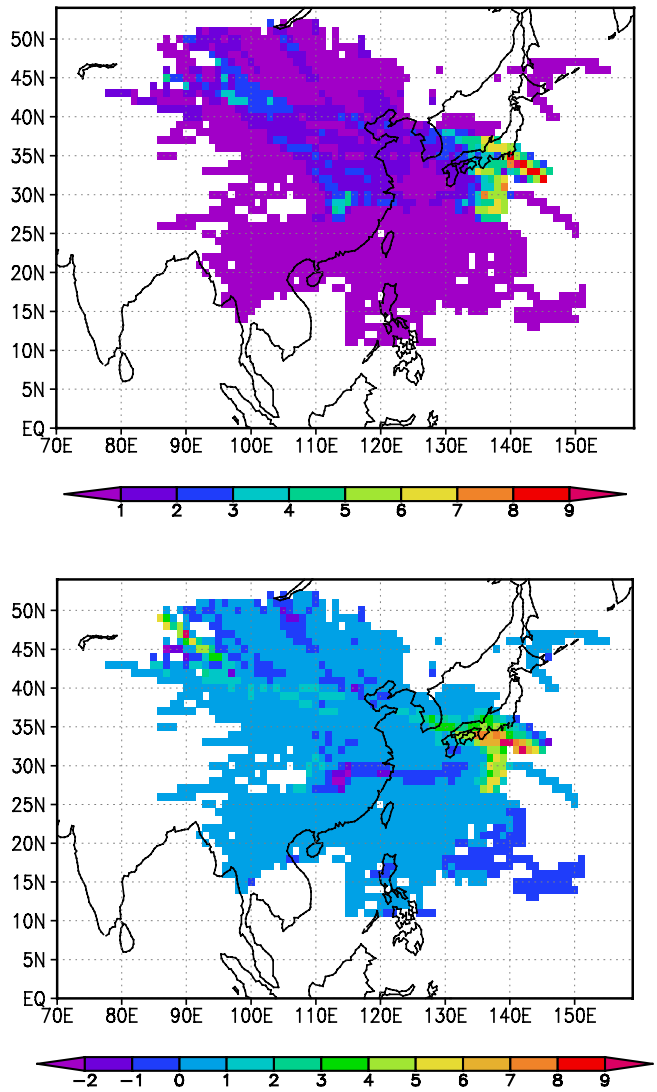

Figure 9. Mission-averaged average distribution of SO_2 below 2 km reconstructed using the aircraft observed values and back-trajectory analysis (upper), and the mean monthly bias between the reconstructed distribution based on the observations and the distribution reconstructed using the modeled values along the flight path (lower). All values are in ppbv.

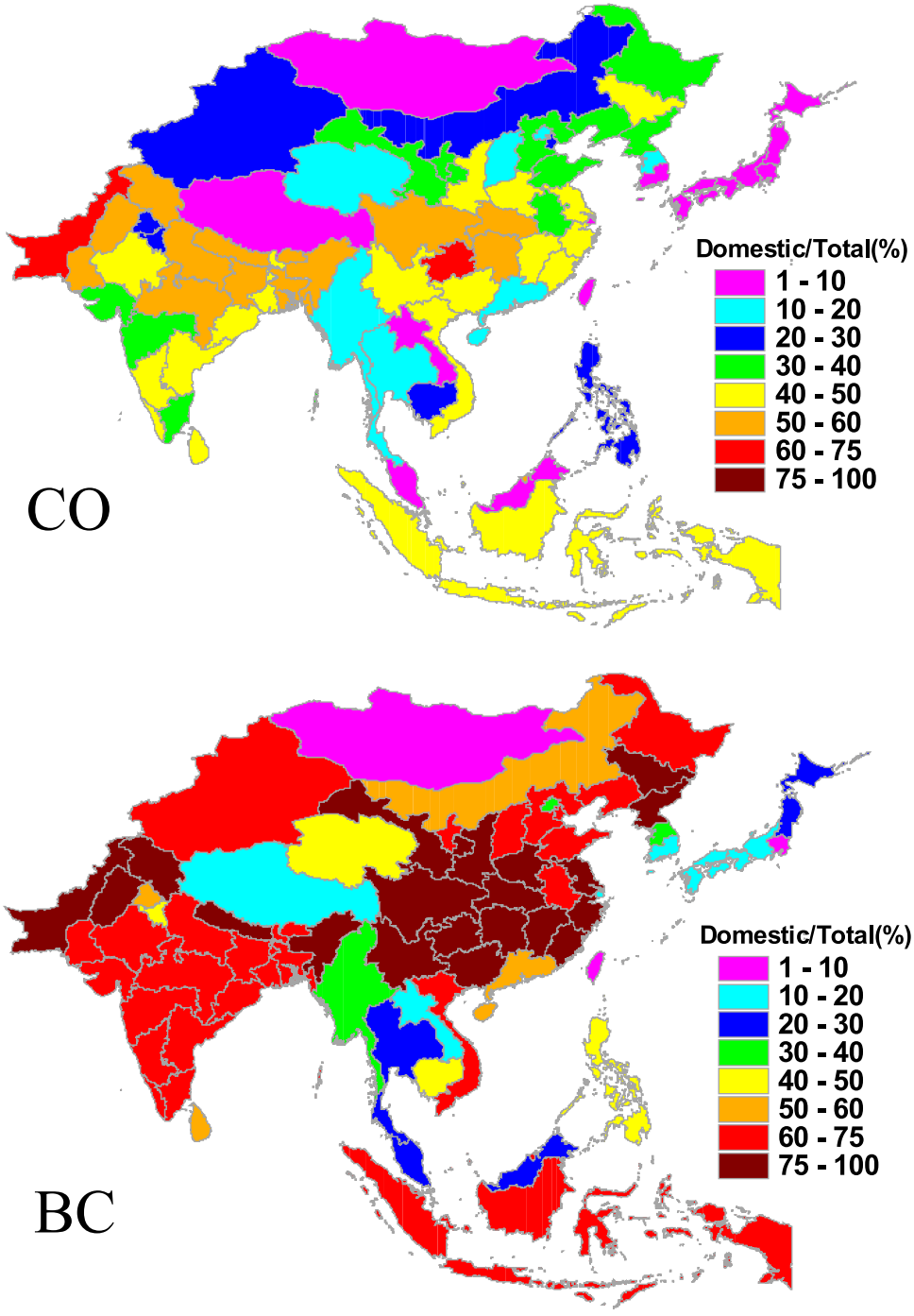

Figure 10. The regional distribution of the contribution of domestic sector emissions of CO and BC expressed as percentage of total emissions.

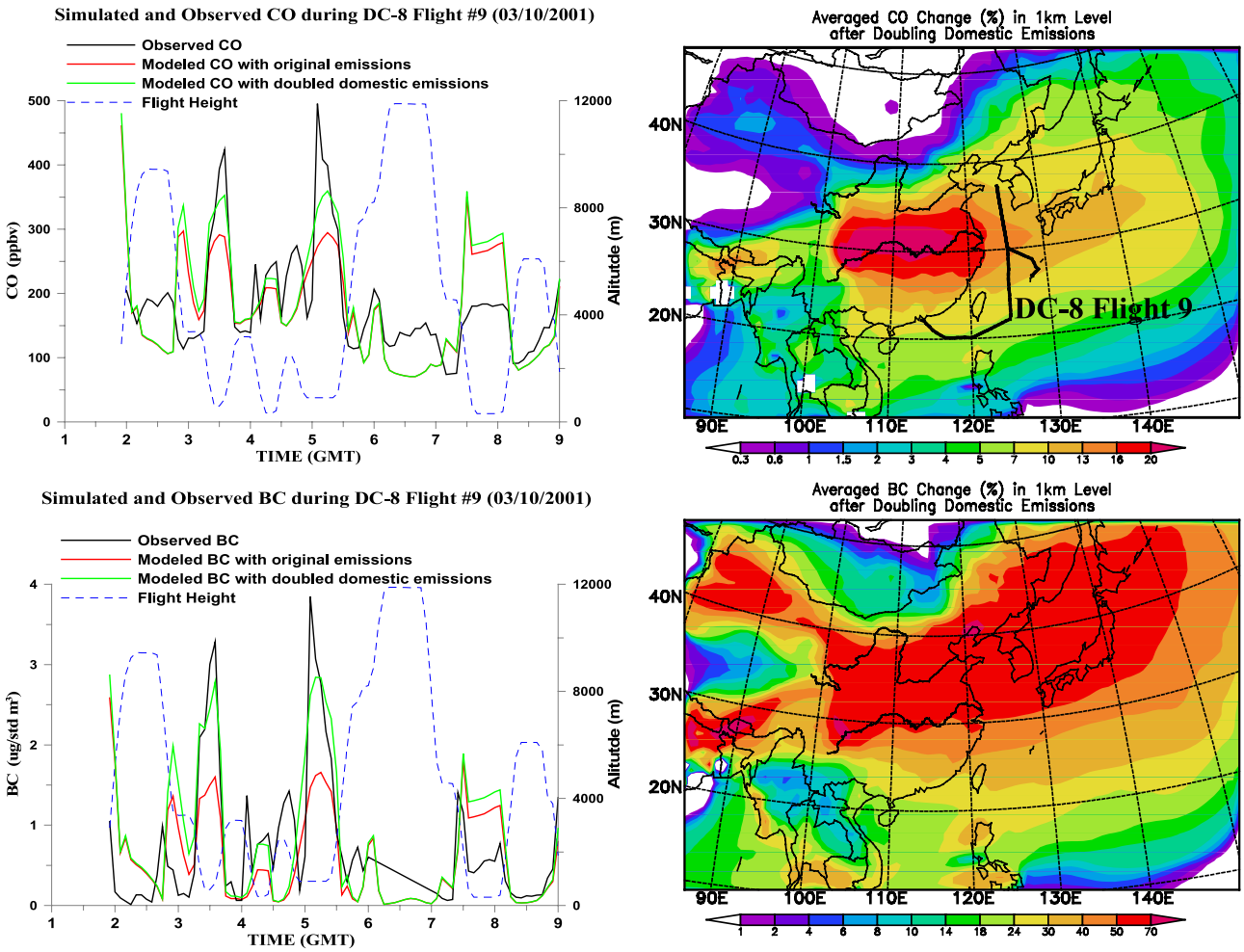

Figure 11. Results from sensitivity simulations using doubled domestic sector emissions. Monthly mean percentage change in near surface CO and BC levels for Asia (right) and along DC-8 flight 9. Flight track is shown.

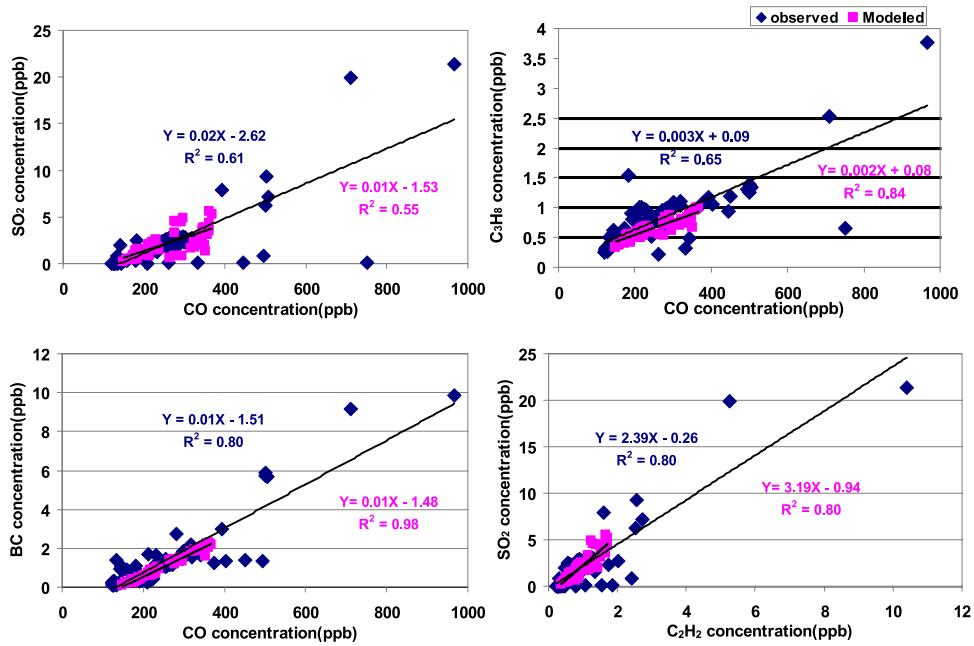

Figure 12. Examples of regression analysis of various species using aircraft observations identified to have encountered Shanghai air masses less than 1 day old (blue). Also shown are values estimated using modeled values for these same data points (pink).